ornl

ORNL/CON-159

OAK RIDGE
NATIONAL
LABORATORY

MARTIN MARIETTA

Development of Advanced Thermal Insulation for Appliances

D. L. McElroy
D. W. Yarbrough
G. L. Copeland
F. J. Weaver
R. S. Graves
T. W. Tong
H. A. Fine

OPERATED BY
MARTIN MARIETTA ENERGY SYSTEMS, INC.
FOR THE UNITED STATES
DEPARTMENT OF ENERGY

Printed in the United States of America. Available from
National Technical Information Service
U.S. Department of Commerce
5285 Port Royal Road, Springfield, Virginia 22161
NTIS price codes—Printed Copy: A05 Microfiche A01

This report was prepared as an account of work sponsored by an agency of the United States Government. Neither the United States Government nor any agency thereof, nor any of their employees, makes any warranty, express or implied, or assumes any legal liability or responsibility for the accuracy, completeness, or usefulness of any information, apparatus, product, or process disclosed, or represents that its use would not infringe privately owned rights. Reference herein to any specific commercial product, process, or service by trade name, trademark, manufacturer, or otherwise, does not necessarily constitute or imply its endorsement, recommendation, or favoring by the United States Government or any agency thereof. The views and opinions of authors expressed herein do not necessarily state or reflect those of the United States Government or any agency thereof.

ORNL/CON-159
Distribution
Category UC-95d

METALS AND CERAMICS DIVISION

DEVELOPMENT OF ADVANCED THERMAL INSULATION FOR APPLIANCES

D. L. McElroy, D. W. Yarbrough, G. L. Copeland, F. J. Weaver,
R. S. Graves, T. W. Tong, and H. A. Fine

NOTICE: This document contains information of a preliminary nature. It is subject to revision or correction and therefore does not represent a final report.

Date Published - July 1984

Prepared for
Office of
Buildings Energy Research and Development

Prepared by the
OAK RIDGE NATIONAL LABORATORY
Oak Ridge, Tennessee 37831
operated by
MARTIN MARIETTA ENERGY SYSTEMS, INC.
for the
U.S. DEPARTMENT OF ENERGY
under Contract No. DE-AC05-84OR21400

CONTENTS

NOMENCLATURE v

ABSTRACT 1

INTRODUCTION 1

ENERGY SAVINGS 2

CONCEPTS EVALUATED 7

HEAT TRANSFER THROUGH FINE PARTICLES 8

CONVECTIVE HEAT TRANSFER 9

CONDUCTIVE HEAT TRANSFER 10

RADIATIVE HEAT TRANSFER 16

MODEL FOR HEAT TRANSFER BY RADIATION AND CONDUCTION 23

THERMAL CONDUCTIVITY MEASUREMENT SYSTEMS 27

ORNL SCREEN TESTER MEASUREMENTS 28

RADIAL HEAT FLOW MEASUREMENTS 32

CONCLUSIONS AND RECOMMENDATIONS 40

ACKNOWLEDGMENTS 41

REFERENCES 42

Appendix A. BRIEF DESCRIPTION OF CONCEPTS FOR PROVIDING HIGH R-VALUES 45

Appendix B. TABULATION OF $E(\lambda)$ FOR FOUR PARTICLES AND VALUES FOR $\overline{C}$. 49

Appendix C. THERMAL CONDUCTIVITY DATA OBTAINED WITH ORNL-3 AND ORNL-4 55

Appendix D. SOURCES OF MATERIALS TESTED 61

NOMENCLATURE

A	Material parameter associated with particle contact resistance, Eq. (9)
$\overline{C}$	Average value of C defined by Eq. (32), m^{-1}
$\overline{C}_p$	Average for particles other than 7-nm-diam SiO_2, m^{-1}
$\overline{C}_{Si}$	Average for 7-nm-diam SiO_2, m^{-1}
C_p	Heat capacity at constant pressure, J/(kg·K)
D	Interparticle spacing, Eq. (20)
d	Particle diameter, m
d_{sp}	Diameter of contact circle, Eq. (10)
E	Extinction coefficient, a function of λ, m^{-1}
$\overline{E}$	Average Value of E, m^{-1}
F	Blackbody function
$F_{\lambda_1-\lambda_2}$	For interval λ_1–λ_2
F_p	Fraction of added particles
F_s	Fraction solid
g	Acceleration of gravity, 9.8 m/s^2
h	Structure parameter equal to $L - l$
k	Thermal conductivity, W/(m·K)
k_a	Apparent
k_c	Of composite
k_g	Of gas phase
k_g°	Of bulk gas at 101 kpa (1 atm)
k_g'	Of gas in porous medium
k_r	Radiative
k_s	Of solid
k_{sp}	Of contact region between spheres
k_k	Coefficient of particle adhesion
k_m	Ratio of particle microroughness to particle diameter/1000
l	Pore size (particle diameter), m
L	Characteristic cell size, m
L°	Thickness, m
L_p	Mean pore size, m

L_g	Mean free path in gas phase, m
m	Refractive index
n	Real part of complex refractive index
N	Number of particles per unit volume, m^{-3}
q_r	Radiant heat flux, W/m^2
Q_{a_λ}	Absorption efficiency, a function of λ
$Q_{s\lambda}$	Scattering efficiency, a function of λ
$Q_{s\lambda}$ eff	Effective value
R	Thermal resistance, $m^2 \cdot K/W$ or $ft^2 \cdot h \cdot {}^\circ F/Btu$
Ra_o	Modified Rayleigh number, Eq. (1)
T	Temperature, K
T_C	Cold surface
T_H	Hot surface
T_m	Modified mean absolute temperature defined by Eq. (30)
w	Imaginary part of refractive index
x	Size parameter, Eq. (21)
α	Absorption coefficient, a function of λ, m^{-1}
β	Coefficient of thermal expansion; is $1/T$ for ideal gases, $3.33 \times 10^{-3}\ K^{-1}$ at 300 K
ε	Emissivity or emittance
ε_C	Of cold surface
ε_H	Of hot surface
κ	Permeability of porous medium, m^2
λ	Wavelength, μm
ν	Kinematic viscosity, m^2/s
ρ	Density, kg/m^3
σ	Stefan-Boltzmann constant, $5.6697 \times 10^{-8}\ W/(m^2 \cdot K^4)$
σ_λ	Scattering coefficient, a function of λ, m^{-1}
τ_λ	Fraction transmitted at wavelength λ
τ°	Optical thickness

DEVELOPMENT OF ADVANCED THERMAL INSULATION FOR APPLIANCES

D. L. McElroy, D. W. Yarbrough, G. L. Copeland, F. J. Weaver,
R. S. Graves, T. W. Tong,* and H. A. Fine*

ABSTRACT

The development of thermal insulation with an apparent thermal conductivity of less than 0.0072 W/(m·K) (equivalent to a thermal resistance per inch thickness of 20 $ft^2 \cdot h \cdot °F/Btu$) is discussed. A theoretical model that includes radiative and conductive heat transfer shows that the target thermal resistance can be attained by combinations of very fine powders and reduced pressures.

Apparent thermal conductivities of fine powders were measured with three apparatuses. A linear heat flow measurement demonstrated apparent thermal conductivities as low as 0.0087 W/(m·K) (*R* per inch = 16.6 $ft^2 \cdot h \cdot °F/Btu$) for evacuated panels containing fine particles. Radial heat flow measurements on fine powders as a function of temperature, gas pressure, and bed density showed that apparent thermal conductivities below the target value can be achieved with pressures below 100 Pa. The radial heat flow measurements also demonstrated the existence of an optimum mass fraction solid in the powder insulations.

INTRODUCTION

Improvements in energy efficiency have been made over the last few years in home and commercial appliances, but loss of energy by heat transfer through appliance insulation remains a significant waste. Appliances for which thermal insulation is particularly important include water heaters, ovens, refrigerators, and freezers. Appliance insulations in common use include polyurethane foam with an *R*-value per inch of about 1.2 $m^2 \cdot K/W$ (7.0 $ft^2 \cdot h \cdot °F/Btu$) for low temperatures and fiberglass with an *R*-value per inch of about 0.5 $m^2 \cdot K/W$ (2.7 $ft^2 \cdot h \cdot °F/Btu$) for high temperatures. Recognizing that substantial energy savings would result if

*University of Kentucky, College of Engineering, Lexington.

appliances could be produced with improved insulation, the Oak Ridge National Laboratory (ORNL) contracted with Arthur D. Little, Inc. (ADL), to determine if insulations with *R*-values per inch of at least 3.5 $m^2 \cdot K/W$ (20.0 $ft^2 \cdot h \cdot °F/Btu$) could be developed and demonstrated.

The ADL study by Lawrence and Ruccia showed that significant energy savings could be realized by increasing the effectiveness of insulation used in appliances.[1] Savings were calculated as a function of insulation *R*-values for several types of appliances. This information allows calculation of payback periods for new insulation systems once their *R*-values and costs are determined.

Several concepts were proposed by ADL for high *R*-value insulation. Most were based on the use of evacuated systems, but some were based on air-filled systems containing very small particles. Thermal conductivity data for many of the systems were not available in the temperature range of interest, so *R*-values could only be estimated. The purpose of this work is to evaluate the thermal performance of the more promising materials and concepts identified by the ADL report. Efforts thus far have been concentrated on systems filled with small particles at atmospheric pressure and under moderate vacuum. The technical feasibility of achieving very high *R*-values with evacuated systems has been demonstrated.[2-5] If, however, sufficiently high *R*-values can be obtained with air-filled systems, manufacturing and lifetime goals of evacuated systems can be more easily achieved.

ENERGY SAVINGS

Energy savings expected to result from the use of improved thermal insulation were calculated for several residential and commercial appliances as a function of the *R*-value of their insulation.[1] These energy savings (Tables 1 and 2) were combined with estimates of manufacturing and materials costs to calculate payback periods (Tables 3 and 4). The concepts evaluated in Tables 3 and 4 are all for evacuated systems except for concept V-2. A detailed discussion of the high *R*-value concepts is contained in the ADL report,[1] and an abbreviated description is contained in

Table 1. Saving from use of improved insulation in residential appliances

Appliance	Energy consumption (kWh/year)	Savings with improved insulation[a]					
		k_a = 0.0144 W/(m·K) R = 10.0[b]		k_a = 0.0096 W/(m·K) R = 15.0		k_a = 0.0072 W/(m·K) R = 20.0	
		(kWh)	($/year)	(kWh)	($/year)	(kWh)	($/year)
Refrigerator	1084	226	11.28[c]	448	22.40	551	27.54
Freezer (chest)	1143	229	11.43	451	22.55	545	27.25
Water heater							
Gas	8994	712	9.23[d]	838	10.87	899	11.67
Electric	5889	445	22.27	486	24.30	512	25.64
Oven							
Gas	826	50	0.64	59	0.77	64.5	0.84
Electric	360	50	2.50	59	2.95	64.5	3.22

[a]Savings at point of use compared with appliance having insulation R-value of 8.

[b]Thermal resistance per inch, $ft^2 \cdot h \cdot °F/Btu$.

[c]Electricity at $0.05/kWh.

[d]Gas at $3.80/$10^6$ Btu.

Source: W. T. Lawrence and F. E. Ruccia, *Development of Advanced Insulation for Appliances. Task I Report*, ORNL/Sub-81/13800/1, June, 1981.

Table 2. Saving from use of improved insulation in commercial appliances

Appliance	Energy consumption (kWh/year)	Savings with improved insulation[a]					
		k_a = 0.0144 W/(m·K) R = 10.0[b]		k_a = 0.0096 W/(m·K) R = 15.0		k_a = 0.0072 W/(m·K) R = 20.0	
		(kWh)	($/year)	(kWh)	($/year)	(kWh)	($/year)
Freezer[c]	674	214	10.69[d]	466	23.29	574	28.71
Water heater							
Gas	1058	688	8.93[e]	809	10.49	870	11.29
Electric	1140	744	37.21	873	43.65	940	47.02
Oven[f]							
Gas	1230	762	9.87	891	11.56	967	12.54
Electric	1230	762	38.09	891	44.53	967	48.34

[a]Savings at point of use compared with appliance having insulation R-value of 8.

[b]Thermal resistance per inch, $ft^2 \cdot h \cdot °F/Btu$.

[c]Three feet of door section for display freezer.

[d]Electricity at $0.05/kWh.

[e]Gas at $3.80/Btu × 10^6.

[f]Single free-standing oven.

Source: W. T. Lawrence and F. E. Ruccia, *Development of Advanced Insulation for Appliances. Task I Report*, ORNL/Sub-81/13800/1, June, 1981.

Table 3. Payback periods for improved insulations in residential appliances

k_a of Insulation [W/(m·K)]	0.0096	0.0072	0.0096	0.0072	0.0072	0.0072	0.0072	0.0072	0.0072	0.0072
R per inch ($ft^2 \cdot h \cdot {}^\circ F/Btu$)	15.0	20.0	15.0	20.0	20.0	20.0	20.0	20.0	20.0	20.0
Insulation concept[a]	IV	VI	IX	X	XI	XII	A	B	C	D
Appliance	Payback (years)									
Refrigerator	6.4	2.4	>7	2.8	>7	>7	>7	>7	>7	>7
Frezers	5.9	2.6	>7	2.9	>7	6.1	4.7	>7	>7	>7
Water heaters										
Gas	7.0	4.9	>7	5.1	>7	>7	4.7	5.0	4.8	4.7
Electric	4.2	2.4	5.4	2.6	4.8	4.4	4.2	>7	5.2	3.0
Ovens										
Gas	>7	>7	>7	*b*	*b*	*b*	*b*	*b*	>7	>7
Electric	>7	>7	>7	*b*	*b*	*b*	*b*	*b*	>7	>7

[a]See Appendix A for descriptions of concepts. All insulations in this table are evacuated.

[b]Temperature range of insulation is not suitable.

Source: W. T. Lawrence and F. E. Ruccia, *Development of Advanced Insulation for Appliances. Task I Report*, ORNL/Sub-81/13800/1, June, 1981.

Table 4. Payback periods for improved insulations in commercial appliances

k_a of Insulation [W/(m·K)]	0.0096	0.0072	0.0072	0.0096	0.0072	0.0072	0.0072	0.0072	0.0072	0.0072	0.0072
R per inch ($ft^2 \cdot h \cdot °F/Btu$)	15.0	20.0	20.0	15.0	20.0	20.0	20.0	20.0	20.0	20.0	20.0
Insulation concept[a]	IV	V-2	VI	IX	X	XI	XII	A	B	C	D
Appliance	Payback (years)										
Display freezers	6.2	>7	1.6	>7	2.2	>7	>7	>7	>7	>7	>7
Water heaters											
Gas	>7	>7	5.9	>7	6.4	>7	>7	>7	>7	>7	>7
Electric	3.4	>7	1.8	4.7	2.0	4.2	3.8	3.6	6.5	4.5	2.5
Ovens											
Gas	5.8	>7	4.3	6.9	*b*	*b*	*b*	*b*	*b*	6.9	4.6
Electric	1.5	4.3	1.1	1.8	*b*	*b*	*b*	*b*	*b*	1.8	1.2

[a]See Appendix A for descriptions of concepts. All insulations in this table are evacuated except concept V-2.

[b]Temperature range of insulation is not suitable.

Source: W. T. Lawrence and F. E. Ruccia, *Development of Advanced Insulation for Appliances. Task I Report*, ORNL/Sub-81/13800/1, June, 1981.

Appendix A. For example, concept VI (perlite powder evacuated to 1 kPa or 0.01 atm) shows a payback of about 2.4 years for residential water heaters using electricity and a payback period of about 1.1 years for commercial ovens using electricity. Tables 3 and 4 include several cases having payback periods of less than 24 months.

CONCEPTS EVALUATED

The development of improved thermal insulations depends on a reduction of gas-phase heat conduction, which can be accomplished by increasing the time or distance traveled between molecular collisions. This can be accomplished by making the effective pore size in the solid media small and thus providing a collision barrier or by decreasing the number density of molecules in the gas by reducing the pressure. The pore-size reduction can be accomplished by using very fine powders so that effective pore size is smaller than the 0.07-μm mean free path for air at atmospheric pressure and room temperature. The mean free path can be greatly increased by evacuating the system because it is inversely proportional to the absolute pressure.[6] The above design concepts and the relative importance of gas conduction, solid conduction, and radiative transport are discussed in following sections.

Four of the most promising design concepts identified by ADL are contained in Table 5. Three of the four systems in Table 5 achieve high thermal resistance through evacuation, and one system, V-2, makes use of a fine powder. Published information on the thermal resistance of an air-filled fine powder approaching the objective of 3.5 $m^2 \cdot K/W$ (20.0 $ft^2 \cdot h \cdot °F/Btu$) per inch appears to be limited to the paper by Verschoor and Greebler.[2] A fine powder system patented by L'Air Liquide[7] claims an *R*-value per inch of about 4.9 $m^2 \cdot K/W$ (28.0 $ft^2 \cdot h \cdot °F/Btu$) for 188 K (−121°F) and air at atmospheric pressure. The 0.0035-μm powder could have a thermal resistance per inch approaching 3.5 $m^2 \cdot K/W$ (20.0 $ft^2 \cdot h \cdot °F/Btu$) at 300 K. Thermal conductivity data from the L'Air Liquide patent, shown as curve 7 in Fig. 1 for 0.0035 μm particles, encouraged efforts to explore relationships between particle size, density, and thermal resistance of evacuated powders.

Table 5. Promising design concepts for high thermal resistance

Concept	V-2	VI	X	XII
Material	Compressed silica powder	Perlite powder	Perlite powder and polyurethane foam	Perlite powder and honeycomb composite
k_a, W/(m·K)	0.0072	0.0072	0.0072	0.0072
Potential *R*-value per inch, ft^2·hr·°F/Btu	20.0	20.0	20.0	20.0
Temperature limit, °C	>300	>300	>65	>200
Cost[b]	22	1.0	1.5	3
Interstitial gas pressure, Pa	1.01×10^5[c]	13	13	13
Leak detector level,[d] cm^3/s at standard conditions	*e*	10^{-8}	10^{-8}	10^{-8}

[a]See Appendix A for descriptions of concepts.

[b]Cost relative to concept I.

[c]Atmospheric pressure.

[d]Leak detector requirement for quality control.

[e]Not applicable.

Source: W. T. Lawrence and F. E. Ruccia, *Development of Advanced Insulation for Appliances. Task I Report*, ORNL/Sub-81/13800/1, June, 1981.

HEAT TRANSFER THROUGH FINE PARTICLES

Heat transfer occurs in the insulation systems of interest by convection, conduction, and radiation in the continuous gas phase and by conduction and radiation in the discontinuous solid phase. An exact description of this very complicated heat transfer process is beyond the scope of this work. Simplified models of the various aspects of the heat transfer are, however, useful in establishing the approximate dependence of the thermal properties of the insulation system on physical properties, such as solid volume fraction and particle size. These models are developed in this section.

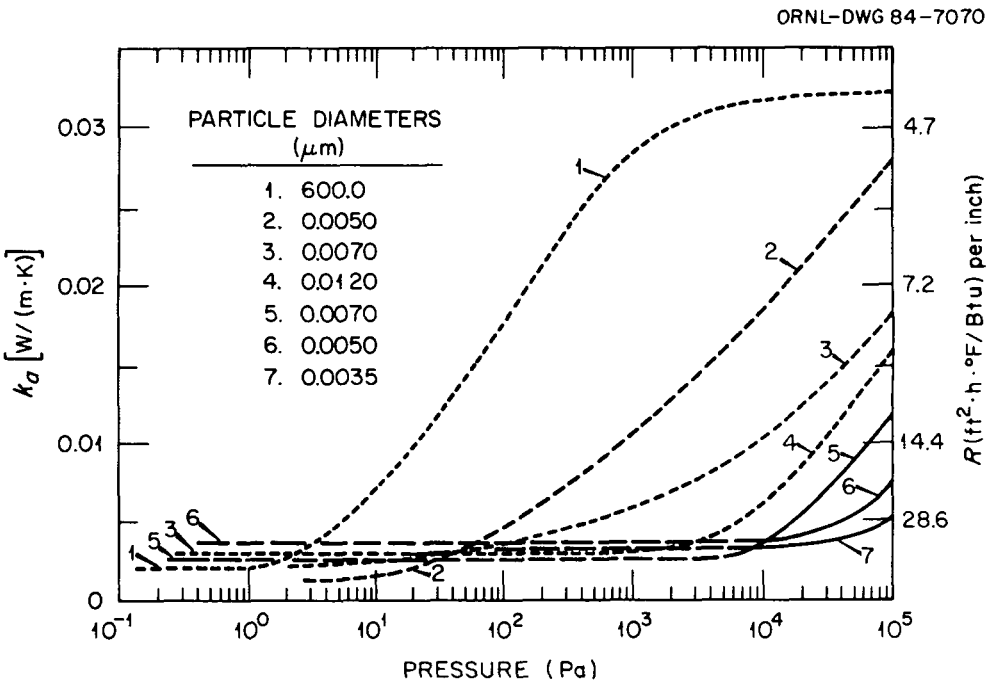

Fig. 1. Thermal conductivity of fine powders at 188 K (−120°F) as a function of pressure. *Source of data*: P. Pellaux-Gervais and D. Goumy, U.S. Patent 4,159,359, June 26, 1979.

CONVECTIVE HEAT TRANSFER

Figure 2 shows that natural convective heat transfer in a vertical porous medium occurs when the modified Rayleigh number divided by the aspect ratio, which is the ratio of vertical height to distance between surfaces, is greater than 4. The modified Rayleigh number is a measure of the buoyancy force relative to the fluid flow resistance due to the presence of the porous material and is defined as

$$Ra_o = g\beta\ \Delta T\ \rho C_p L\kappa / \nu k_c\ . \tag{1}$$

For most insulation systems, all the variables* in Eq. (1) are well defined except the permeability of the porous medium κ and the thermal conductivity of the composite k_c. If we assume typical values for the other variables Eq. (1) becomes

$$Ra_o = \frac{(9.8)(3.3\times10^{-3})(40)(1.16)(1000.0)(0.0254)}{(15.87\ \times\ 10^{-6})}\ \frac{\kappa}{k_c} = 2.42\ \times\ 10^{6}\kappa/k_c\ . \tag{2}$$

*See Nomenclature.

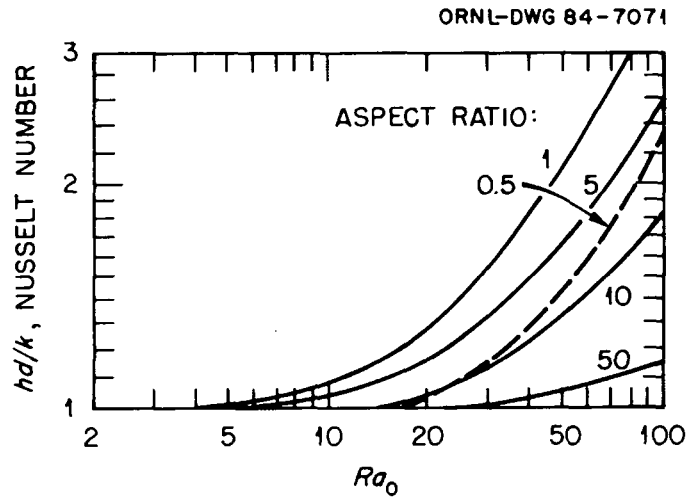

Fig. 2. The material convective heat transfer calculated numerically for permeable space with isothermal vertical and insulated horizontal boundaries for different aspect ratios.

Known values of κ for typical insulations having a solid fraction around 0.1 range from 10^{-8} to 10^{-10} m^2 (ref. 8). If k_e is taken to be 10^{-2} W/(m·K), then Ra_o is in the range 0.024 to 2.4. The Nusselt number is defined as the ratio of the effective thermal conductivity with convection to the effective thermal conductivity without convection; for this range of Ra_o, calculations by Bankvall[8] show a Nusselt number of 1, which corresponds to no heat transfer by natural convection. This is the case for aspect ratios from 0.5 to 50 shown in Fig. 2.

For horizontal insulation heated from below, Lapwood[9] established the criterion for the onset of fluid motion as

$$Ra_o > 4\pi^2 \ . \tag{3}$$

From the above estimate for Ra_o, we see that under typical conditions Ra_o is smaller than $4\pi^2$ and that the contribution of natural convection to heat transfer is usually negligible in horizontal insulation.

CONDUCTIVE HEAT TRANSFER

A review identifying many of the proposed models for conductive heat transfer in porous media is given by Crane, Vachon and Khader.[10] These

models, as well as the vast majority of the previous work, focus on materials with large volume fraction solids. The materials of interest in this work, however, are mostly gas with less than 0.2 volume fraction solids.

The method of generalized conductivities was used by Luikov et al. to develop a model for conductive heat transfer in the gas and solid phases of porous granular systems.[11] The model was shown to yield accurate predictions by Luikov et al.[11] for many materials and by Rogers and Williamson[12] for materials very similar to those of interest in this work. This model will therefore be used to describe conduction in the gas and solid phases.

According to Luikov et al.,[11] the thermal conductivity of a composite material equals

$$k_c = \frac{k_s}{(h/L)^{-2} + A} + (1 - h/L)^2 k_g + \frac{2k_g}{(k_g/k_s)(1 + h/l) + (h/L)^{-1}} , \qquad (4)$$

where h, l, and $L = h + l$ are parameters that characterize the structure of the solid skeleton in the composite and are related to the fraction solid by

$$F_s = 3(h/L)^2 - 2(h/L)^3 . \qquad (5)$$

The length L is for the edge of a simple cubic cell with a particle center at each corner and is the distance between particle centers. The thickness of the rectangular elements that approximate the cell volume occupied by solid is denoted h, and l is the distance between solid elements. When the conductivity of the gas is much less than that of the solid, the second and third terms of Eq. (4) may be combined to yield

$$k_c = \frac{k_s}{\dfrac{1}{(h/L)^2} + A} + [1 + (h/L)^2] k_g . \qquad (6)$$

The quantity h/L is always less than 1, and for small values of h/L the cubic term in Eq. (5) will be much smaller than the quadratic term, so

$$(h/L)^2 = F_s/3 \ . \tag{7}$$

Combining Eqs. (6) and (7) yields

$$k_c = 0.33F_s k_s/(1 + 0.33F_s A) + (1 + 0.33F_s)k_g \ . \tag{8}$$

The term A equals the ratio of the conductivity of the solid phase to that through the point contact and microgap between two spherical particles in contact and is approximated by

$$A = 1/[k_{sp}/k_s + (250k_g^{\circ}/k_s k_k k_m)(h/L)^2] \ , \tag{9}$$

$$k_{sp}/k_s = d_{sp}/d \ . \tag{10}$$

Material constants k_k and k_m are defined by Luikov et al.;[11] d_{sp} is the diameter of the circle of contact when two spheres of diameter d are pressed together. The manufacturing technique for the ultrafine powders used in the insulation systems under discussion results in physical contact between particles. If one envisions two particles bonded together forming an hourglass shape, the ratio d_{sp}/d will equal the ratio of the diameter of the neck of the hourglass to the diameter of the upper or lower bulb. This ratio will have a characteristic value for the material.

The second term in the denominator of Eq. (9) contains the ratio of the conductivity of the gas in the microgap between two adjacent spheres to that of the pure solid. The microgap will be an order of magnitude smaller than an individual sphere. Thus, if ultrafine spheres are used as insulation, the microgaps will be several orders of magnitude smaller than the mean free path of the gas molecules. Kistler[13] and Verschoor and Greebler[2] have shown that conductivity of a gas in a porous medium equals

$$k_g^{\circ} = k_g^{\circ} L_p/(L_p + L_p) \ . \tag{11}$$

For very small particles yielding very small microgaps, the second term in the denominator of Eq. (9) will be small compared with the first term, and A will equal d/d_{sp}, a material constant ranging from 1 to ∞.

Finally, because the pores in the materials of interest will be smaller than the mean free path of the gas molecules, k_g in Eq. (8) must be replaced by the value obtained from Eq. (11), with the mean pore size L_p (ref. 2) given by

$$L_p = 2d/3F_s \ . \tag{12}$$

Equations (8), (9), (11), and (12) are combined to yield a model for the thermal conductivity of the composite:

$$k_c = \frac{0.33F_s k_s}{1 + 0.33AF_s} + \frac{(1 + 0.33F_s)k_g^\circ}{1 + 1.5L_gF_s/d} \ . \tag{13}$$

The dependence of k_c on F_s for values of A ranging from 10 to 1000, L_g/d of 7 and 700, and a gas phase at atmospheric pressure are shown in Fig. 3. The solid conductivity for these calculations was 1.38 W/(m·K), the value for fused silica at 300 K, and k_g° was 0.026 W/(m·K), the value for air at 300 K (ref. 14). Clearly, both A and L_g/d have an important effect on the thermal conductivity of the composite. Increasing A by a factor of 100 and L_g/d from 7 to 700 decreases k_c by a factor ranging from 10 to 30. Furthermore, the results in Table 6 show that, although A must be large to reach the project goal of k_c = 0.0072 W/(m·K) (R per inch = 20 ft^2·h·°F/Btu), L_g/d must also be on the order of 100. Increasing L_g/d

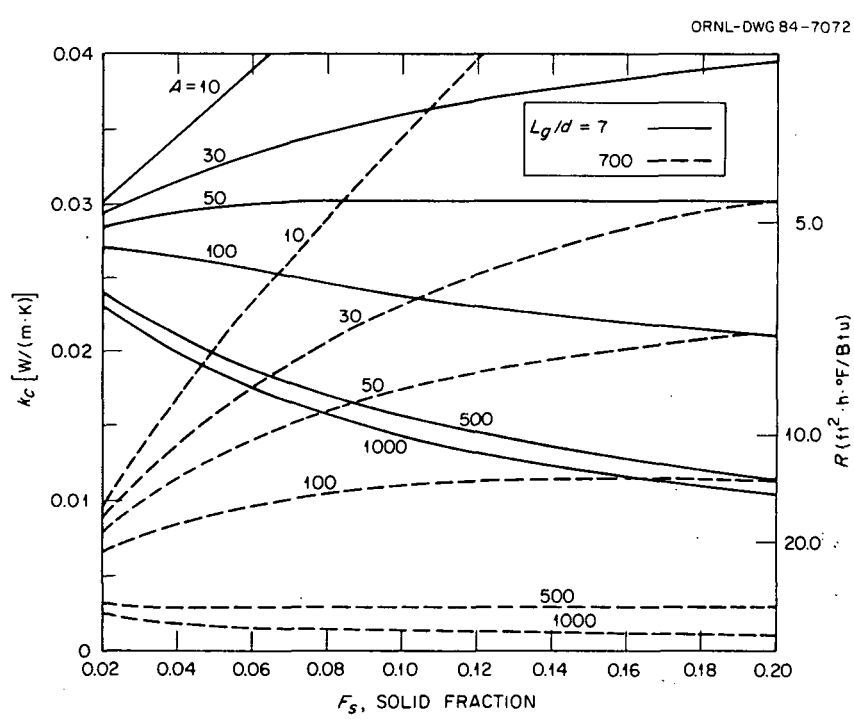

Fig. 3. Calculated thermal conductivities of insulations with small solid fractions. R-values on right scale are for 25.4-mm-thick (1-in.) material.

Table 6. Calculated dependence of the gas and solid conduction components of the apparent thermal conductivity of the composite on the ratio L_g/d

[k_s = 1.38 W/(m·K) and k_g° = 0.026 W/(m·K)]

F_s	L_g/d	k_c [W/(m·K)]		
		A = 10	A = 100	A = 1000
0.04	7×10^0	0.0346	0.0264	0.0198
	7×10^1	0.0212	0.0129	0.0063
	1.4×10^2	0.0189	0.0107	0.0041
	2.1×10^2	0.0180	0.0098	0.0032
	3.5×10^2	0.0173	0.0090	0.0025
	7×10^2	0.0167	0.0085	0.0019
	7×10^4	0.0161	0.0079	0.0013
	7×10^6	0.0161	0.0079	0.0013
0.10	7×10^0	0.0473	0.0237	0.0144
	7×10^1	0.0366	0.0129	0.0037
	1.4×10^2	0.0355	0.0118	0.0026
	2.1×10^2	0.0351	0.0114	0.0022
	3.5×10^2	0.0347	0.0111	0.0018
	7×10^2	0.0345	0.0108	0.0016
	7×10^4	0.0342	0.0106	0.0013
	7×10^6	0.0342	0.0106	0.0013
0.20	7×10^0	0.0638	0.0209	0.0103
	7×10^1	0.0561	0.0132	0.0026
	1.4×10^2	0.0555	0.0126	0.0020
	2.1×10^2	0.0553	0.0124	0.0018
	3.5×10^2	0.0551	0.0122	0.0016
	7×10^2	0.0550	0.0121	0.0015
	7×10^4	0.0549	0.0120	0.0014
	7×10^6	0.0549	0.0120	0.0014

above 700 by reducing the pressure or by using smaller particles has, however, little effect on k_c. For example, if F_s is 0.10 and A is 10, then increasing L_g/d from 700 to 7×10^6 causes k_c to decrease from 0.0345 to 0.0342 W/(m·K).

As shown in Table 7, a decrease in k_g° yields a decrease in the composite thermal conductivity k_c. In addition, as one increases A

Table 7. Calculated dependence of the gas and solid conduction components of the apparent thermal conductivity on the gas conductivity[a]

F_s	k_g° [W/(m·K)]	k_c [W/(m·K)]		
		A = 10	A = 100	A = 1000
0.04	2.60	0.0774	0.0691	0.0625
	0.26	0.0222	0.0140	0.0074
	0.026	0.0167	0.0085	0.0019
	0.0026	0.0163	0.0079	0.0013
0.10	2.60	0.0596	0.0359	0.0267
	0.26	0.0368	0.0131	0.0039
	0.026	0.0345	0.0108	0.0016
	0.0026	0.0343	0.0106	0.0014
0.20	2.60	0.0680	0.0251	0.0145
	0.26	0.0562	0.0133	0.0027
	0.026	0.0550	0.0121	0.0015
	0.0026	0.0549	0.0120	0.0014

[a] k_s = 1.38 W/(m·K) and L_g/d = 700.

from 10 to 1000, further decreases in k_c are predicted. The result of increasing the fraction solid is interdependent on A and L_g/d.

A cross plot of some of the values in Tables 6 and 7 is given in Fig. 4. The results indicate that in principle a gas with a high k_g° can be used to give a small k_c as long as its L_g is also large. For example, if k_g° is 0.026 W/(m·K) and L_g/d is 7, a k_c of 0.0237 W/(m·K) is predicted. If k_g° and L_g/d are simultaneously increased to 0.26 W/(m·K) and 700, respectively, then a k_c of 0.0131 W/(m·K) is predicted. Although this is theoretically possible, it is not practical at room temperature and atmospheric pressure because no known gas has k_g° of 0.26 W/(m·K) under these conditions.

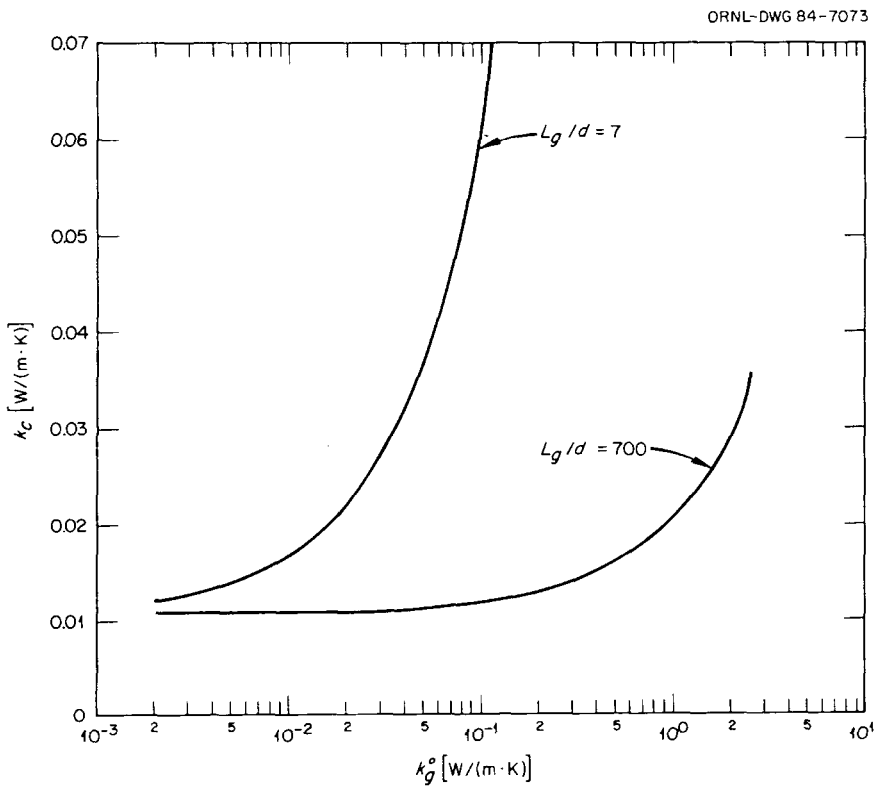

Fig. 4. The dependence of k_c on k_g^o for two values of L_g/d with A = 100, F_s = 0.1, and k_s = 1.38 W/(m·K).

Finally, the effect of solid conductivity on the conductivity of the composite is shown in Table 8. For most of the cases considered, reduction of k_s by a factor of 2 will cause a corresponding reduction in k_c. For example, a reduction in k_s from 1.38 to 0.69 W/(m·K) will reduce k_c from 0.0108 to 0.0056 W/(m·K) for F_s = 0.1 and A = 100.

RADIATIVE HEAT TRANSFER

Thermal radiation traversing a porous material is attenuated through absorption and scattering by the solid phase and absorption by the gas. If the gas is transparent as in the case of N_2 or O_2, then absorption and scattering by the solid predominate.

The extinction coefficient is the parameter that characterizes the attenuation of radiation as a function of wavelength λ (ref. 15). It is defined as the sum of the absorption α_λ and scattering σ_λ coefficients:

$$E(\lambda) = \alpha_\lambda + \sigma_\lambda \ . \tag{14}$$

Table 8. Calculated dependence of the gas and solid conduction components of the apparent thermal conductivity on the solid conductivity[a]

F_s	k_s [W/(m·K)]	k_c [W/(m·K)]		
		A = 10	A = 100	A = 1000
0.04	1.38	0.0167	0.0085	0.0019
	0.69	0.0087	0.0045	0.0013
	0.345	0.0046	0.0026	0.0009
0.10	1.38	0.0345	0.0108	0.0016
	0.69	0.0174	0.0055	0.0009
	0.345	0.0088	0.0029	0.0006
0.20	1.38	0.0550	0.0121	0.0015
	0.69	0.0276	0.0061	0.0008
	0.345	0.0138	0.0031	0.0005

[a] k_g° = 0.026 W/(m·K) and L_g/d = 700.

Extinction coefficients for fine powder insulations of interest in this study are calculated in this section. These results are then used to establish the dependence of radiative heat transfer on material properties.

The extinction coefficient for a material containing N spherical isotropic particles per unit volume is given by

$$E(\lambda) = (N\pi d^2/4)(Q_{a\lambda} + Q_{s\lambda}) \ , \tag{15}$$

where $Q_{a\lambda}$ and $Q_{s\lambda}$ are the absorption and scattering efficiencies, respectively. Since

$$F_s = N\pi d^3/6 \ , \tag{16}$$

the extinction coefficient can be expressed as a function of the volume fraction solid

$$E(\lambda) = 3(Q_{a\lambda} + Q_{s\lambda})F_s/2d \ . \tag{17}$$

If particles are far apart then $Q_{a\lambda}$ and $Q_{s\lambda}$ can be calculated according to the Mie formulation, which assumes independent scattering by the particles.[16] When the particles are close enough to exhibit dependent scattering, $Q_{s\lambda}$ must be replaced by an effective scattering efficiency $Q_{s\lambda}$ eff, while no correction may be needed for $Q_{a\lambda}$ (ref. 17). Assuming rhombohedral random particle spacing, Brewster and Tien[17] suggested that, when

$$D/\lambda < 0.3 \ , \tag{18}$$

$Q_{s\lambda}$ eff can be obtained from Hottel et al.'s correlation[18]

$$\log_{10} \log_{10}(Q_{s\lambda}/Q_{s\lambda}\ \text{eff}) = 0.25 - 5.1(D/\lambda) \ . \tag{19}$$

In Eqs. (18) and (19), D is the surface-to-surface interparticle spacing for rhombohedral packing:

$$D = (0.905/F_s^{1/3} - 1)d \ . \tag{20}$$

Even if dependent scattering exists, the Mie efficiencies $Q_{a\lambda}$ and $Q_{s\lambda}$ must clearly first be calculated to determine $E(\lambda)$. The Mie efficiencies are functions of the material properties[16] such as the size parameter

$$x = \pi d/\lambda \ , \tag{21}$$

and the complex refractive index

$$m = n - iw \ . \tag{22}$$

Once $Q_{a\lambda}$ and $Q_{s\lambda}$ are available, $Q_{s\lambda}$ eff can be calculated from Eq. (19) whenever condition (18) is met for a given F_s, and $E(\lambda)$ can be calculated from Eq. (17).

Figure 5 shows $E(\lambda)$ for three SiO_2 particle sizes and one size of carbon particle. Values of $E(\lambda)$ are tabulated in Appendix B. In the calculations for fused silica, values of n and w were taken from Champetier and Friese[19] for wavelengths between 7 and 26 μm. Values for the real part n were taken from the *American Institute of Physics Handbook*[20] for wavelengths below 7 μm. The imaginary part w was calculated from transmission data given by DeWitt.[14] The fraction transmitted through a sample of thickness $L°$ is

$$\tau_\lambda = \exp(-4wL°/\lambda) \ . \tag{23}$$

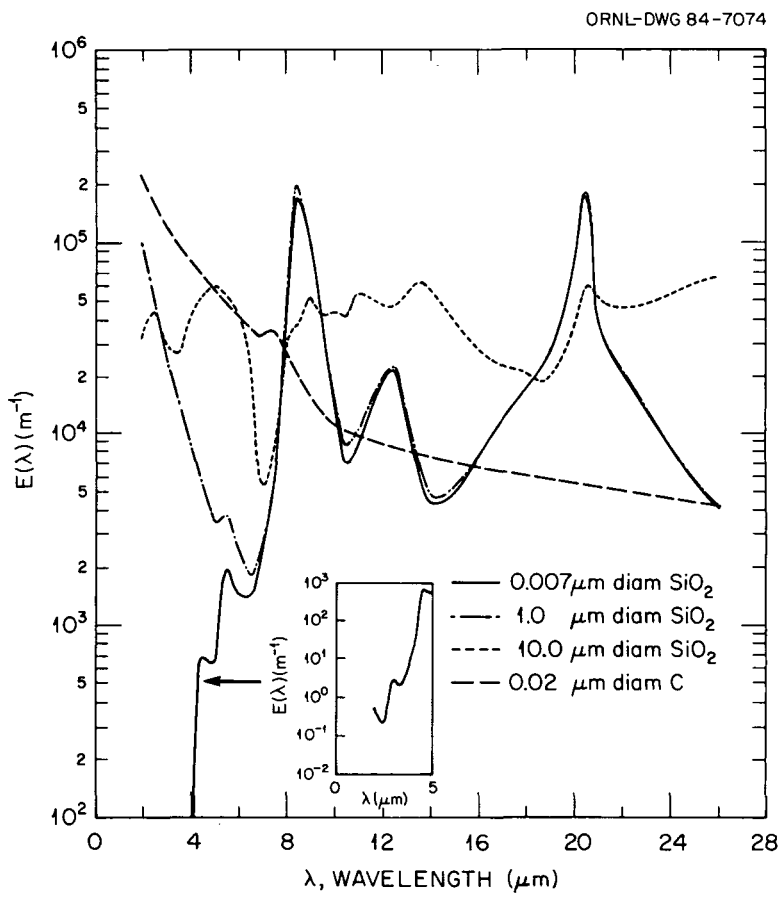

Fig. 5. Calculated extinction coefficients for four powder systems at F_s = 0.1.

The results for carbon particles were obtained from values for n and ω reported by Foster and Howarth.[21] The results in Fig. 5 show that $E(\lambda)$ for the 0.0070-μm-diam fused silica is much smaller in the short wavelengths than in the long wavelengths. This trend is, however, not observed for the micron-size fused silica or for the 0.02-μm-diam carbon particles. For the 0.02-μm carbon particles, the $E(\lambda)$ curve above λ = 10 μm is based on n and ω values at 10 μm. As discussed earlier, particles with low thermal conductivity and large L_g/d are required to reduce conduction. This makes angstrom-size silica particles the most suitable material for achieving the project goal of R per inch = 20 ft^2·h·°F/Btu. The optical thickness of a medium of physical thickness $L°$ is

$$\tau° = EL° \ . \tag{24}$$

Samples consisting of angstrom-size silica particles at $F_S = 0.1$ will therefore have optical thicknesses less than 0.1 at $L°$ of 25.4 mm and wavelengths less than 3.5 μm. The same samples will have large optical thicknesses at longer wavelengths. To minimize radiative heat transfer, it is desirable to have large optical thicknesses at all wavelengths with significant energy. The results in Fig. 5 suggest that mixing micron-size silica particles or 0.02-μm carbon black with angstrom-sized silica will give large optical thicknesses at all wavelengths. In light of the above observations, the effects of particle size and solid volume fraction on radiative transport can be estimated.

The diffusion approximation can be used to calculate the radiant heat flux through a sample with large optical thickness.[22-23] For one-dimensional heat transfer across a material bounded by isothermal parallel plates at temperatures T_H and T_C, the radiant heat flux equals

$$q_r = \sigma(T_H^4 - T_C^4)/(3EL°/4 + 1/\varepsilon_H + 1/\varepsilon_C - 1) \ . \tag{25}$$

A mean value for E, $\overline{E}$, should be used when the extinction coefficient is wavelength dependent. This mean value is weighted by the Planck function[24] to account for the amount of energy at a given wavelength.

Equation (25) is valid only when the material has a large optical thickness at all wavelengths that contain significant energy. The radiant heat flux will equal

$$q_r = \sigma(T_H^4 - T_C^4)/(1/\varepsilon_H + 1/\varepsilon_C - 1) \ , \tag{26}$$

when the optical thickness is small. Equation (26) applies when $E(\lambda)L°$ is small for all wavelengths with significant energy.

When large and small optical thickness regimes exist, such as the case with angstrom-size silica particles, a wavelength-dependent solution to the transfer equation must be used to get an exact solution.[22] An additive solution based on Eqs. (25) and (26) can, however, be used to find an approximate heat flux. The total radiant flux in this case is

$$q_r = \frac{F_{\lambda_1-\lambda_2}\sigma(T_H^4 - T_C^4)}{1/\varepsilon_H + 1/\varepsilon_C - 1} + \frac{(1 - F_{\lambda_1-\lambda_2})\sigma(T_H^4 - T_C^4)}{3\overline{E}L°/4 + 1/\varepsilon_H + 1/\varepsilon_C - 1} \ , \tag{27}$$

where $F_{\lambda_1-\lambda_2}$ is the fraction of radiant energy in the interval λ_1 to λ_2, the region of low optical thickness, and $\overline{E}$ is the average value for E outside the interval $\lambda_1-\lambda_2$. An apparent radiation conductivity k_r can be defined such that

$$q_r = k_r(T_H - T_C)/L^\circ \ . \tag{28}$$

Combination of Eqs. (27) and (28) yields

$$k_r = \frac{4F_{\lambda_1-\lambda_2}\sigma T_m{}^3 L^\circ}{1/\varepsilon_H + 1/\varepsilon_C - 1} + \frac{4(1 - F_{\lambda_1-\lambda_2})\sigma T_m{}^3 L^\circ}{3\overline{E}L^\circ/4 + 1/\varepsilon_H + 1/\varepsilon_C - 1} \ , \tag{29}$$

where

$$T_m = [(T_H{}^4 - T_C{}^4)/4(T_H - T_C)]^{1/3} \ . \tag{30}$$

The first term on the right-hand side of Eq. (29) is due to radiation that shines directly through the insulation. When Eq. (29) is applied to the angstrom-size silica with λ_1 and λ_2 taken as 0 and 3.5 μm, respectively, the importance of the shine-through component in the equation can be estimated. Table 9 contains results for the two components in Eq. (29) for four values of F_s. The results show that, at T_m = 300 K, the shine-through component could account for about half the radiation conductivity and that, above T_m = 500 K, it dominates. Clearly, the shine-through component must be eliminated if the desired apparent thermal conductivity of 0.0072 W/(m·K) is to be reached.

The shine-through component can be eliminated by adding a material that will increase the optical thickness in the 0- to 3.5-μm wavelength region. Carbon black, 1-μm-diam silica particles, or 10-μm diam-silica particles can be used for this purpose because their $E(\lambda)$ are large in the short wavelengths.

Equation (17) can be used to represent the averaged extinction coefficient as a function of F_s:

$$\overline{E} = \overline{C}F_s \ , \tag{31}$$

$$\overline{C} = (3/2)(\overline{Q}_a + \overline{Q}_s)/d \ . \tag{32}$$

Table 9. Dependence of k_r on temperature for 25.4-mm-thick material bounded by black planes

T_m (K)	$F_{0-3.5\ \mu m}$ [a]	$\frac{F_{0-3.5\ \mu m} \cdot 4\sigma T_m^3 L^\circ}{1/\varepsilon_H + 1/\varepsilon_C - 1}$ [W/(m·K)]	$\frac{(1 - F_{0-3.5\ \mu m}) \cdot 4\sigma T_m^3 L^\circ}{3\bar{E}L^\circ/4 + 1/\varepsilon_H + 1/\varepsilon_C - 1}$ [W/(m·K)]			
			$F_s = 0.02$	$F_s = 0.04$	$F_s = 0.1$	$F_s = 0.2$
300	0.562×10^{-3}	0.000087	0.001807	0.000909	0.000365	0.000183
500	0.0337	0.024312	0.008850	0.004454	0.001788	0.000895
700	0.15072	0.297791	0.031320	0.015810	0.006359	0.003185
900	0.30694	1.288924	0.081842	0.041505	0.016745	0.008397

[a]Source: R. Siegel and J. R. Howell, *Thermal Radiation Heat Transfer*, 2d ed., McGraw-Hill, New York, 1972, pp. 739–46.

When a different type of particle is mixed with the angstrom-size silica, $\overline{E}$ can be determined by

$$\overline{E} = [\overline{C}_p F_p + \overline{C}_{Si}(1 - F_p)]F_s \ , \tag{33}$$

where subscript p signifies particles other than the angstrom-size silica, Si denotes the angstrom-size silica, and

$$F_p = \frac{\text{particle volume other than the angstrom-size silica}}{\text{total solid volume}} \ . \tag{34}$$

The effects of mixing 95 vol % angstrom-size silica and 5 vol % of either 0.02-μm carbon black, 1-μm silica, or 10-μm silica on the radiation conductivity are shown in Table 10. In determining k_r for the mixtures considered, the shine-through term in Eq. (29) was dropped by taking $F_{\lambda_1-\lambda_2}$ equal to zero. This can be done because the 25.4-mm-thick insulations are optically thick at all wavelengths once any of the aforementioned particles are mixed with 0.0070-μm silica. The values of $\overline{C}_{Si}$ and $\overline{C}_p$ used in the calculations appear in Appendix B. These illustrations clearly show that at T_m = 300 K the effect of adding a material to reduce shine-through is small but that the effect of mixing increases with temperature and reduces the radiant heat flux. The amount that is added will, however, increase the volume fraction solid and the solid thermal conductivity of the composite. The existence of an optimum composition is suggested by the model that has been introduced.

MODEL FOR HEAT TRANSFER BY RADIATION AND CONDUCTION

The total heat flux through the insulations being discussed is approximately equal to the sum of the conductive and net radiative heat fluxes. If the two heat transfer mechanisms are taken to be uncoupled, then the upper limit of the apparent thermal conductivity can be written as

$$k_a = k_c + k_r \ . \tag{35}$$

Equation (13) for k_c and (29) for k_r discussed in the preceeding sections can be used in Eq. (35) to give a model for the apparent thermal

Table 10. Effect on apparent radiation contribution to thermal conductivity from mixing 7.0-nm-diam silica with 5 vol % other particles

Additive		k_r [W/(m·K)] from Eq. (29) at each T_m (K)			
Other material	Particle diameter (μm)	300	500	700	900
		$F_s = 0.02$			
None		0.00189	0.03317	0.3291	1.3708
Carbon black	0.02	0.00185	0.00892	0.03228	0.08741
Silica	1.0	0.00180	0.00909	0.03583	0.10901
Silica	10.0	0.00176	0.00881	0.03398	0.10264
		$F_s = 0.04$			
None		0.00099	0.02877	0.3136	1.3304
Carbon black	0.02	0.00093	0.00449	0.01627	0.04416
Silica	1.0	0.00091	0.00457	0.01808	0.05522
Silica	10.0	0.00089	0.00443	0.01714	0.05196
		$F_s = 0.10$			
None		0.00045	0.02610	0.3041	1.3057
Carbon black	0.02	0.00037	0.00180	0.00654	0.01778
Silica	1.0	0.00036	0.00184	0.00727	0.02227
Silica	10.0	0.00036	0.00178	0.00689	0.02094
		$F_s = 0.2$			
None		0.00027	0.02521	0.3010	1.2973
Carbon black	0.02	0.00019	0.00090	0.00328	0.00891
Silica	1.0	0.00018	0.00092	0.00364	0.01116
Silica	10.0	0.00018	0.00089	0.00345	0.01049

conductivity from which the total heat flux can be calculated. The steps required to obtain $k_a < 0.0072$ W/(m·K) (R per inch = 20 h·ft^2·°F/Btu) can be summarized as follows:

1. particle-to-particle contact must be minimized (large A),
2. solids with low thermal conductivity should be used,
3. the ratio L_g/d should be made as large as possible by using either small particles (small d) or evacuation (large L_g) or both to obtain a particle-to-particle spacing less than the mean free path in the gas phase,

4. direct radiative transport (shine-through) must be eliminated, and
5. the gas phase conductivity must be low.

Equations (13) and (29) can be combined to provide a predictive model for k_a that can be used to demonstrate property combinations that have k_a < 0.0072 W/(m·K) at T_m = 300 K. Table 11 contains examples of such combinations, which show the magnitudes required for L_g/d and A to obtain the target thermal conductivity with 0.007-μm silica. Table 12 contains property combinations that yield k_a in the range 0.0072 to 0.0144 W/(m·K) (R-value per inch ranging from 10 to 20 ft^2·h·°F/Btu).

Table 11. Property combinations having k_a < 0.0072 W/(m·K)[a] at T_m = 300 K and atmospheric pressure

F_s	L_g/d	A	k_c[b]	k_r[c]	k_a
0.02	700.0	250.0	0.004627	0.00181	0.0064
	400.0	500.0	0.004131	0.00181	0.0059
	200.0	1000.0	0.004937	0.00181	0.0067
	400.0	1000.0	0.003212	0.00181	0.0050
0.04	400.0	250.0	0.005290	0.000996	0.0063
	100.0	500.0	0.006160	0.000996	0.0072
	400.0	500.0	0.003451	0.000996	0.0045
	200.0	500.0	0.004423	0.000996	0.0054
0.10	100.0	250.0	0.006602	0.000452	0.0071
	200.0	250.0	0.005790	0.000452	0.0062
	400.0	250.0	0.005364	0.000452	0.0058
	600.0	250.0	0.005218	0.000452	0.0057
	1000.0	250.0	0.005101	0.000452	0.0056
0.20	50.0	250.0	0.006937	0.000270	0.0072
	100.0	250.0	0.006099	0.000270	0.0064
	200.0	250.0	0.005659	0.000270	0.0059
	500.0	250.0	0.005434	0.000270	0.0057
	600.0	250.0	0.005358	0.000270	0.0056

[a]Thermal resistance per inch 20 ft^2·h·°F/Btu.

[b]k_c values calculated by use of k_g° = 0.026 W/(m·K) and k_s = 1.38 W/(m·K).

[c]k_r is based on 0.0070-μm SiO_2 particles.

Table 12. Property combinations having $0.0072 < k_a < 0.0144$ W/(m·K)[a] at T_m = 300 K and atmospheric pressure

F_s	L_g/d	A	k_c[b]	k_r[c]	k_a
0.02	200.0–700.0	10.0	0.01228–0.009734	0.00181	0.0115–0.0141
	200.0–1000.0	30.0	0.011341–0.008447	0.00181	0.0103–0.0132
	200.0–1000.0	50.0	0.010587–0.007692	0.00181	0.0095–0.0124
	100.0–1000.0	100.0	0.012030–0.006331	0.00181	0.0081–0.0138
	100.0–400.0	250.0	0.009980–0.005450	0.00181	0.0073–0.0118
	50.0–200.0	500.0	0.012587–0.005857	0.00181	0.0077–0.0144
	50.0–1000.0	1000.0	0.011667–0.007741	0.00181	0.0096–0.0135
0.04	200.0–1000.0	50.0	0.013000–0.011405	0.000996	0.0124–0.0140
	100.0–1000.0	100.0	0.011615–0.008940	0.000996	0.0099–0.0126
	100.0–200.0	250.0	0.008000–0.006263	0.000996	0.0073–0.0090
	50.0	500.0	0.008983	0.000996	0.0100
	50.0	1000.0	0.007869	0.000996	0.0089
0.10	100.0–1000.0	100.0	0.012269–0.010769	0.000452	0.0112–0.0127
	50.0–100.0	250.0	0.008083–0.006602	0.000452	0.0071–0.00085
	10.0	500.0	0.013345	0.000452	0.0138
	10.0	1000.0	0.012083	0.000452	0.0125
0.20	100.0–1000.0	100.0	0.012878–0.012076	0.000270	0.0123–0.0131
	10.0–50.0	250.0	0.012134–0.006937	0.000270	0.0072–0.0124
	7.0–10.0	500.0	0.011619–0.009608	0.000270	0.0099–0.0199
	7.0–10.0	1000.0	0.010300–0.008288	0.000270	0.0086–0.0106

[a]Thermal resistance per inch 10–20 ft^2·h·°F/Btu.

[b]k_c values calculated by use of k_g° = 0.026 W/(m·k) and k_s = 1.38 W/(m·K).

[c]k_r is based on 0.0070-μm SiO_2 particles.

Equation (35) shows k_a to be the sum of two terms, both of which depend on F_s. An increase in F_s decreases k_r and the thermal conductivity of the gas phase but increases transport through the solid phase except at very large A values. There should therefore exist an optimum F_s that will minimize the k_a. Figure 6 suggests a minimum in the k_a curve for a selected set of parameters.

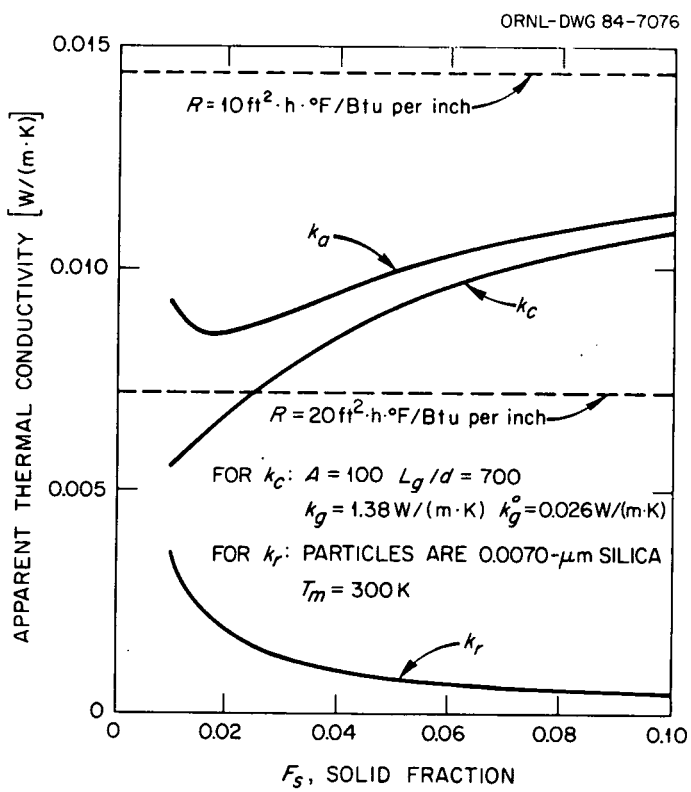

Fig. 6. Calculated apparent thermal conductivity for a 25.4-mm-thick sample as a function of solid fraction.

THERMAL CONDUCTIVITY MEASUREMENT SYSTEMS

The preceeding analysis suggests that high thermal resistance can be achieved by proper design of a very fine particle material or reduction of gas phase conduction by evacuating the region that serves as insulation. Thermal conductivity measurements are still required, however, because the structural parameters cannot be determined from theory, commercially available particles do not have the same shape or packing as the particles in the model, and the degree to which the model describes an actual system must be determined.

Two thermal conductivity measuring methods were used to obtain data for fine-particle materials. A rectangular unguarded screen tester diagrammed in Fig. 7 and described in detail elsewhere[25-27] was used to

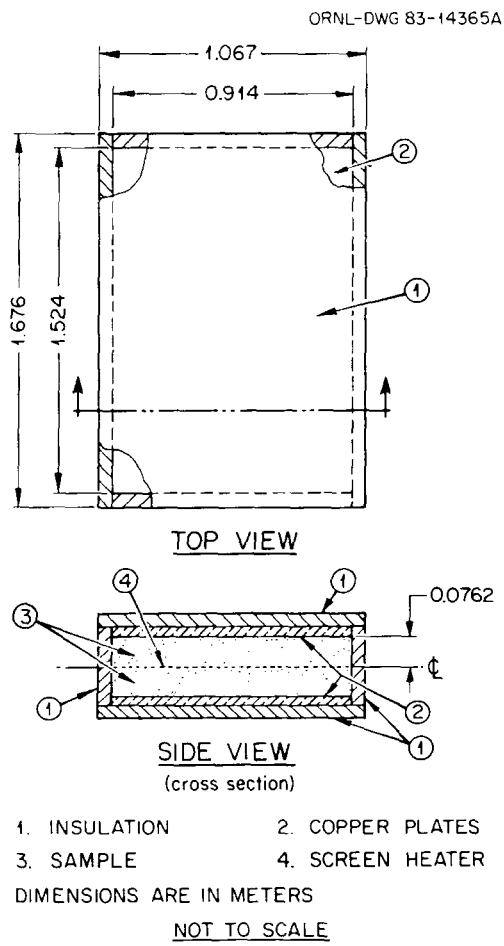

Fig. 7. Diagram of the ORNL unguarded screen tester.

measure the apparent thermal conductivity of an evacuated fine-particle-filled panel (Fig. 8). Radial heat flow was measured to obtain the apparent thermal conductivity k_a of fine particles procured in bulk. Figures 9 and 10 are schematics of the two radial systems, ORNL-3 and ORNL-4, used in this project.

ORNL SCREEN TESTER MEASUREMENTS

The ORNL unguarded screen tester was used to measure the apparent thermal conductivity of National Bureau of Standards (NBS) standard reference material (SRM) 1450-b and a fiberglass batt Certified Transfer Standard with results that were within ±1% of those obtained by NBS (ref. 27). A determinate error analysis showed that apparent thermal

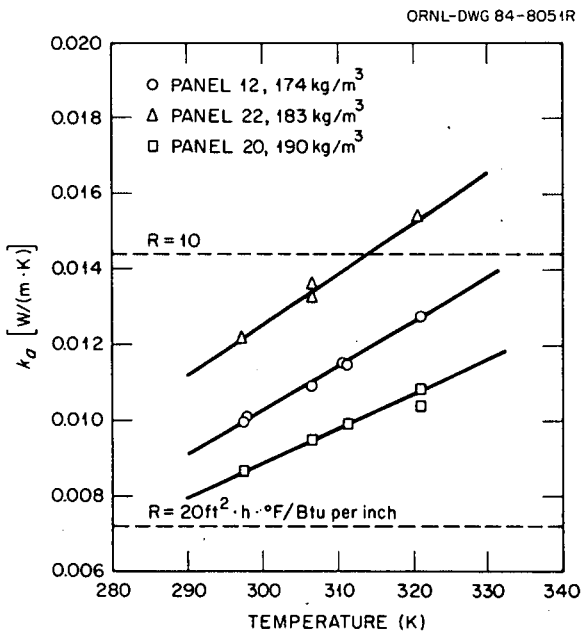

Fig. 8. Measured apparent thermal conductivity for three evacuated panels containing nominally 0.007-μm particles.

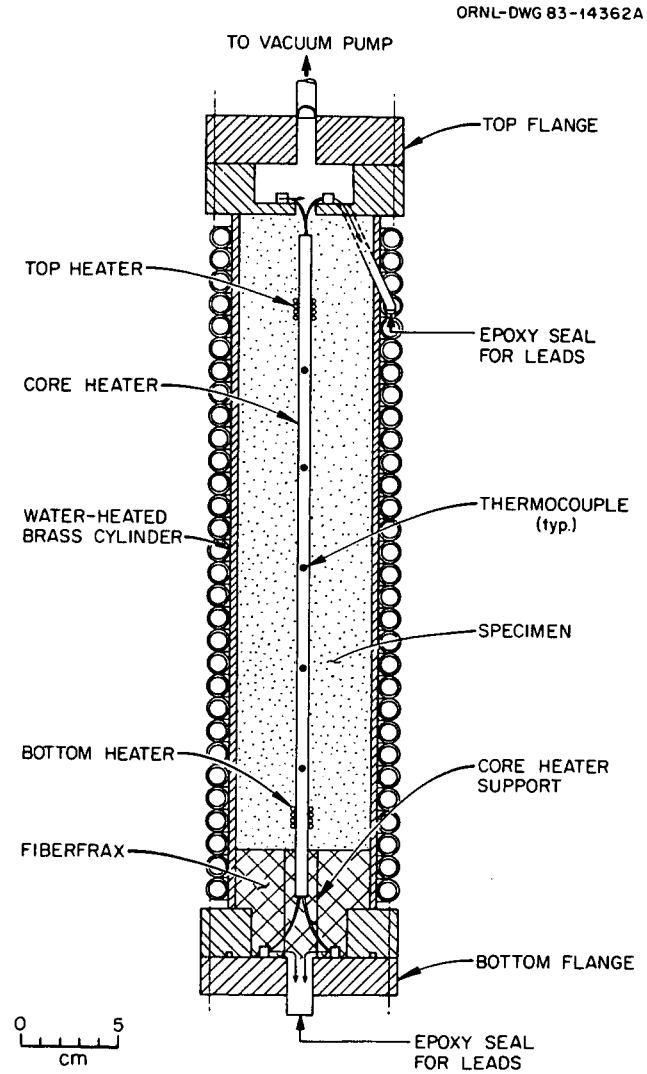

Fig. 9. Schematic of ORNL-3, a guarded radial heat flow apparatus for testing powders.

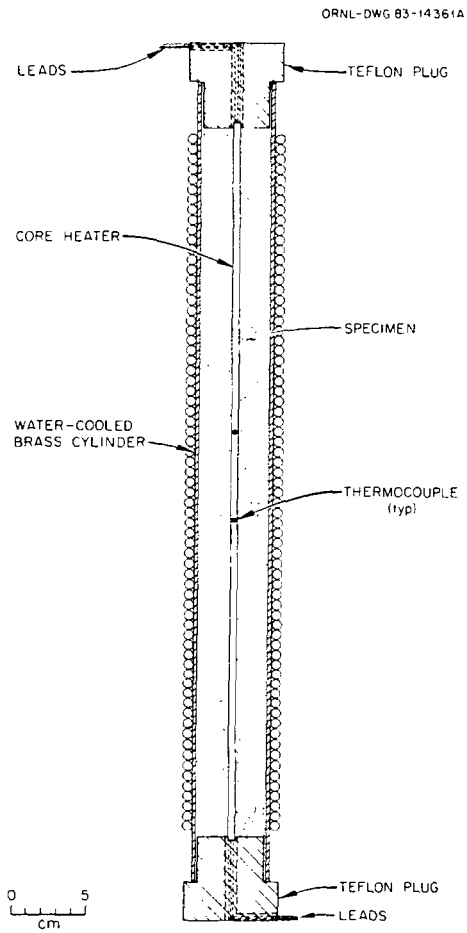

Fig. 10. Schematic of ORNL-4, an unguarded radial heat flow apparatus for testing powders.

conductivities can be measured to better than ±1.5% with the apparatus. The screen tester was used to measure k_a of three fine-particle-filled evacuated rectangular panels[28] that were manufactured by L'Air Liquide.*

The L'Air Liquide panels tested were about 0.97 m (38 in.) long, 0.48 m (19 in.) wide, and 55 mm (2.2 in.) thick and were encased in aluminized plastic. The rectangular panels were filled with Degussa nominally 0.0070-μm-diam fumed silica, evacuated to about 133 Pa (1-mm Hg), and heat sealed. Because the encapsulating material has a finite air permeability, the internal pressure of the panels will increase slowly with time. The panel pressure was estimated to be in the 1.3-to 2.6-kPa range at the time of measurement.[28] Panel characteristics and k_a results in the temperature

*Rectangular evacuated panels filled with fine powder. Panels were fabricated by L'Air Liquide, 57 Avenue Carnot, 94500 Champigny-S/Marne, Paris, France.

range from 297 to 322 K were reported by Copeland et al.;[28] they are reproduced in Table 13 and shown graphically in Fig. 8. The results in Table 13 can be described to better than ±2% by a linear function of temperature with the coefficients indicated in Table 14. These coefficients were used to interpolate a k_a value for each panel at 300 K, and Table 14 shows these to range from 0.0088 W/(m·K) for Panel 20 to 0.0125 W/(m·K) for Panel 22. The corresponding R-values per inch range from 16.3 to 11.6 ft^2·h·°F/Btu and average about 70% of the target thermal resistance at a modest vacuum. The k_a data for the panels increase with temperature and show between panels variations that are likely due to pressure differences as well as density differences. A direct comparison of these results with the theoretical model discussed earlier was not attempted because the panel pressure is uncertain. The k_a results in Table 13 are about four times the value of 0.0025 W/(m·K) reported by L'Air Liquide[7] at a mean temperature of 188 K. If the linear equations given in Table 14

Table 13. Apparent thermal conductivity results for three evacuated panels produced by L'Air Liquide

Panel	Density (kg/m^3)	Dimensions (m)	Mean temperature (K)	k_a [W/(m·K)]
12	174	0.96 × 0.48 × 0.053	297.24	0.00993
			297.78	0.01007
			306.57	0.01090
			310.56	0.01150
			311.02	0.01143
			321.03	0.01277
22	183	0.975 × 0.485 × 0.057	297.31	0.01208
			306.54	0.01321
			306.62	0.01358
			320.60	0.01535
20	190	0.975 × 0.480 × 0.055	297.45	0.00865
			306.79	0.00946
			311.30	0.00953
			321.07	0.01084
			321.22	0.01033

Table 14. Coefficients derived from a least-squares data fit for panels 12, 22 and 20

	Panel 12	Panel 22	Panel 20
Density, g/cm^3	0.174	0.183	0.190
$k_a = A + BT$(K) W/(m·K)			
A	−0.02468	−0.02963	−0.01553
$B \times 10^3$	0.11641	0.14034	0.08117
Average deviation (%)	0.60	0.69	1.68
k_a at 300 K, W/(m·K)	0.01024	0.01247	0.00882
R per inch	14.08	11.56	16.35
$k_a = CT^3$			
C $\times 10^9$	0.3815	0.4630	0.3223
k_a (300 K), W/(M·K)	0.01030	0.01250	0.0087

are extrapolated, they yield negative k_a values below about 200 K. If one assumes that the increase in k_a with temperature is primarily due to radiative heat transfer, then an alternative representation of the panel results with a cubic temperature function may be in order. If this is done and the L'Air Liquide value is included, then the cubic coefficients given in Table 14 describe the results in Table 13 on the three panels as well as does the linear data fit. This cubic fit has the advantage of avoiding negative k_a values. The resulting coefficients in Table 14 are about four times those observed for fibrous carbon insulation[30] and about 60% of that needed to describe the radiation contribution of a typical fiberglass batt at 300 K.

RADIAL HEAT FLOW MEASUREMENTS

The apparent thermal conductivity of a number of commercially available fine powders was tested with the radial heat flow apparatuses ORNL-3 and ORNL-4. The ORNL-3 apparatus (Fig. 9) was constructed to have top and bottom heaters to guard against axial heat flow but was operated in some cases without power to the guard heaters for the measurements being reported. The ORNL-4 apparatus (Fig. 10) is similar to ORNL-3 but without guard heaters. Both ORNL-3 and ORNL-4 were thermally modeled by

use of HEATING5 (ref. 29) to determine the effect of axial heat flow by conduction on measured k_a. Selected results from the thermal modeling effort for no end guarding are shown in Fig. 11. The input data for the HEATING5 calculations are listed in Table 15. The numerical results show that the measured apparent thermal conductivity assuming no axial heat flow is about 5% high for specimens having k_a = 0.0070 W/(m·K) and heater thermal conductivity of 15.0 W/(m·K) when radial temperature difference is determined on the center plane. Increasing k_a to 0.04 W/(m·K) reduces the error to less than 1%. The radial apparatuses have physical dimensions close to those used in the modeling, and the HEATING5 results should be representative of their performance. Apparent thermal conductivity

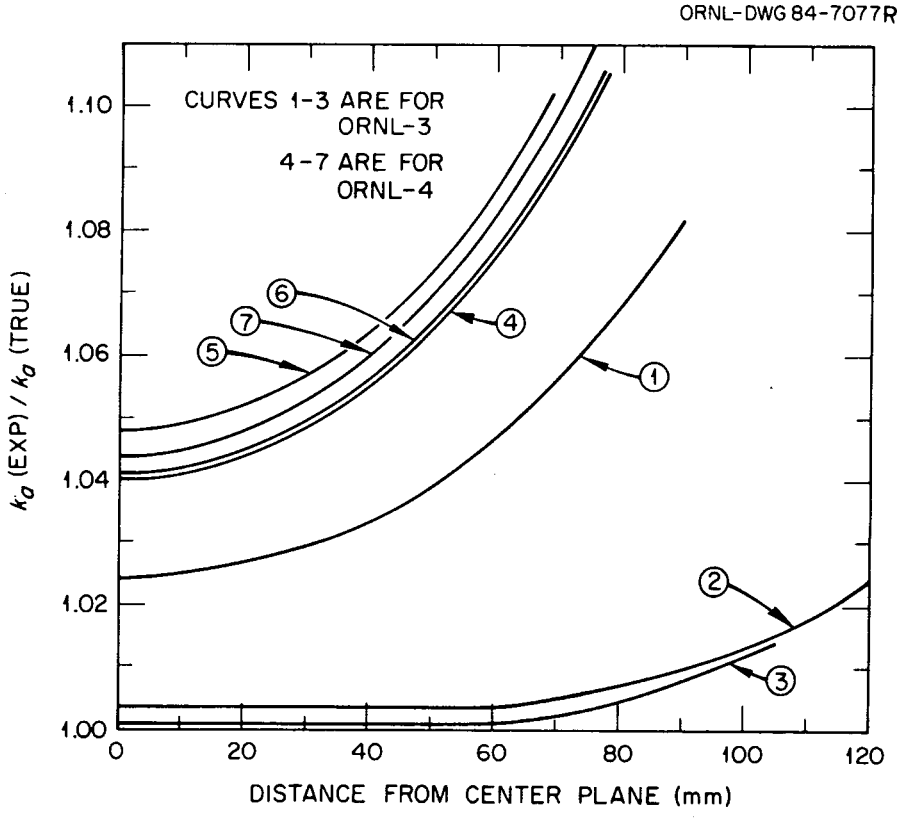

Fig. 11. Thermal modeling results for ORNL-3 and ORNL-4 showing effect of axial heat transfer on measured apparent thermal conductivity. Variables are given in Table 15.

Table 15. Variable specification for HEATING5 calculations for radial apparatuses

Curve (Fig. 11)	Apparatus[a]	Thermal conductivity [W(m·K)]			Maximum ΔT[b] (K)
		Sample	Heater	End plugs	
1	ORNL-3	0.007	15.0		17.50
2	ORNL-3	0.040	0.2		3.06
3	ORNL-3	0.040	0.2		3.06
4	ORNL-4	0.007	15.0	0.2	17.50
5	ORNL-4	0.007	15.0	0.4	17.50
6	ORNL-4	0.007	15.0	0.4	35.00
7	ORNL-4	0.007	15.0	0.2	35.00

[a]Heater tube, inner radius 2.794 mm, outer radius 3.048 mm; specimen, outer radius 15.875 mm, half length 240 mm.

[b]Expected in radial direction with negligible axial losses.

measurements made with ORNL-3 and ORNL-4 were further validated by k_a values obtained on 500-μm Al_2O_3 particles at atmospheric pressure. A comparison of ORNL-3 and ORNL-4 results for the k_a of Al_2O_3 with results obtained with a large guarded radial apparatus shows agreement to better than ±5% (ref. 28).

Apparent thermal conductivities obtained for 15 powders at 300 K and atmosphere pressure with ORNL-4 are shown in Tables 16 and 17. Apparent thermal conductivities for six powders were measured as a function of pressure with ORNL-3. The k_a data at 300 K and atmospheric pressure with ORNL-3 are reported in Table 18. A complete tabulation of the k_a data is contained in Appendix C. In each case k_a was obtained as a function of temperature in the range 298 to 340 K. The k_a data at 300 K were calculated from a least-squares fit of the data to a linear expression in temperature. The entries in Table 16 are grouped with large particles at the top, relatively expensive particles second, and inexpensive commerical material third. Table 17 includes data for two mixtures and Table 18 for one mixture.

Table 16. Apparent thermal conductivities of fine particles at 300 K and atmospheric pressure measured with ORNL-4

	Material[a]	Density (kg/m^3)	Medium	F_s	k_a [W/(m·K)]	R per inch ($ft^2 \cdot h \cdot °F/Btu$)
3	500-μm Al_2O_3 spheres	2395	N_2		0.2736	0.53
9	20–200-μm Cenosphere	368	N_2		0.1114	1.29
1	0.0070-μm Cab-O-Sil S-17	280	Air	0.127	0.0229	6.30
10	Degussa Aerosil 500	54	N_2	0.025	0.0259	5.57
		80	N_2	0.035	0.0231	6.24
2	0.0120-μm Degussa R-974	366	Air		0.0250	5.77
1	0.0070-μm Cab-O-Sil S-17	99	N_2	0.045	0.0233	6.19
		181	N_2	0.082	0.0213	6.77
		280	N_2	0.127	0.0218	6.62
		496	N_2	0.225	0.0416	3.47
11	Microsilica (95%)	273	N_2		0.0359	4.02
12	Microsilica (88%)	238	N_2		0.0328	4.40
4	SiO_2 Selma Gray	242	N_2	0.110	0.0343	4.21
		312	N_2	0.141	0.0357	4.04
		468	N_2	0.212	0.0415	3.48
5	SiO_2 Beverly mixed fume	195	N_2	0.089	0.0318	4.54
6	SiO_2 Ferroalloys	464	N_2	0.211	0.0451	3.20
7	SiO_2 Selma White	209	N_2	0.095	0.0399	3.61
8	SiO_2 Reynolds fume-1	382	N_2	0.174	0.0415	3.48
13	SiO_2-Fe_2O_3 mixture	232	N_2		0.0328	4.39

[a]Additional information on materials is in Appendix D, keyed to the item numbers listed.

Table 17. Apparent thermal conductivities of fine particle mixtures measured with ORNL-4 at 300 K in nitrogen at atmospheric pressure

	Content vol %		Density (kg/m^3)	k_a [W/(m·K)]	R per inch ($ft^2 \cdot h \cdot °F/Btu$)
	Philblack S-212 Carbon Black	Cab-O-Sil			
14	50 vol % Philblack S212, carbon black, and 50 vol % Cab-O-Sil S-17		233	0.0385	3.75
15	5 vol % Philblack S212, carbon black, and 95 vol % Cab-O-Sil S-17		76.6	0.0289	4.99
			360	0.0277	5.21
			360	0.0265	5.44

Table 18. Apparent thermal conductivities of fine particles at 300 K and atmospheric pressure measured with ORNL-3

	Material[a]	Medium	Density (kg/m^3)	k_a [W/(m·K)]	R per inch ($ft^2 \cdot h \cdot °F/Btu$)
3	500-μm Al_2O_3 spheres	Air	2277	0.281	0.51
1	0.0070-μm Cab-O-Sil S-17	N_2	81	0.0287	5.03
18	3M Microspheres	N_2	88.7	0.0383	3.77
4	SiO_2 Selma Gray	N_2	164	0.0369	3.91
5	SiO_2 Beverly mixed fume	N_2	182	0.0342	4.22
17	Perlite	Air	146	0.0558	2.58
16	Mixture of Cab-O-Sil S-17 and 3M microspheres	Air	97	0.0359	4.02

[a]Materials are described in Appendix D.

As expected, the highest thermal resistances at 300 K and atmospheric pressure were observed for the very fine powder systems (Materials 1, 2, 10). The data for Materials 1 and 2 were used to construct the curve shown in Fig. 12. Six data points were described to better than ±3% by a least-squares fit that yielded

$$k_a = 0.1484 \times 10^{-2} + 0.0514\rho + 0.1795 \times 10^{-2}/\rho \ . \qquad (36)$$

The data point for Cab-O-Sil S-17 near 0.5 g/cm^3 was not included in this fit because it seems anomalously high. Equation (36) indicates a minimum k_a of about 0.0207 W/(m·K) (R per inch = 6.97 ft^2·h·°F/Btu) at a density of 0.2 g/cm^3 or an F_s of 0.09. In addition, the data for Degussa Aerosil 500 below a density of 0.1 g/cm^3 suggest an even lower k_a, which is reasonable because this material has a nominal particle diameter of 5 nm, whereas

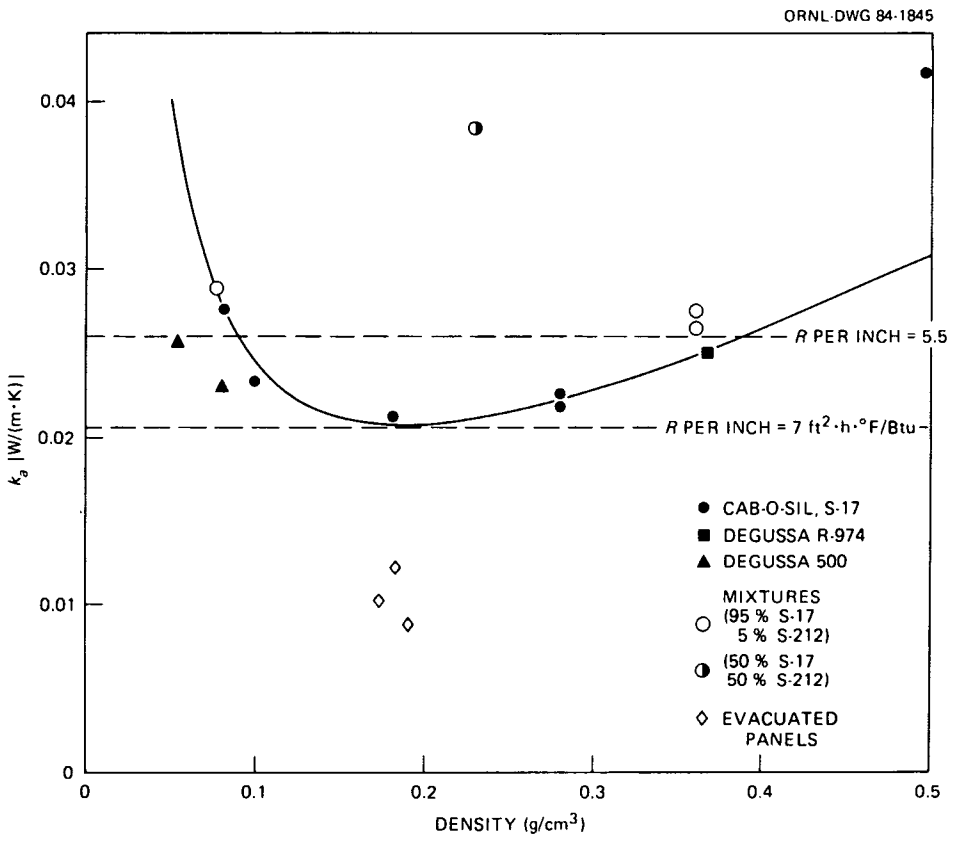

Fig. 12. Apparent thermal conductivity at 300 K and atmospheric pressure as a function of density for Materials 1, 2, and 10 and for two mixtures of silica with carbon black. Evacuated panel k_a values are included.

Materials 1 and 2 have nominally 7- and 12-nm-diam particles. These data support the model introduced earlier that indicates the existence of an optimum F_s or density.

Table 17 shows results obtained for mixtures of 7.0-nm Cab-O-Sil S-17 and Philblack S212 carbon black. The carbon black was added to reduce the radiative component of heat transfer through the powder. The change in k_a is not dramatic for the mixtures contaning 5 vol % carbon black because the total energy being transferred by radiation is thought to be small. The addition of 50 vol % carbon particles increased the heat transfer, and this may be because the particles are more conductive. Figure 12 includes the k_a values given in Table 14 for the three evacuated panels that are formed from nominally 10-nm-diam particles. The k_a values for the evacuated material are about half of the projected minimum k_a in air.

The data at 300 K and atmospheric pressure for inexpensive commerical materials is shown as a function of density in Fig. 13. These materials

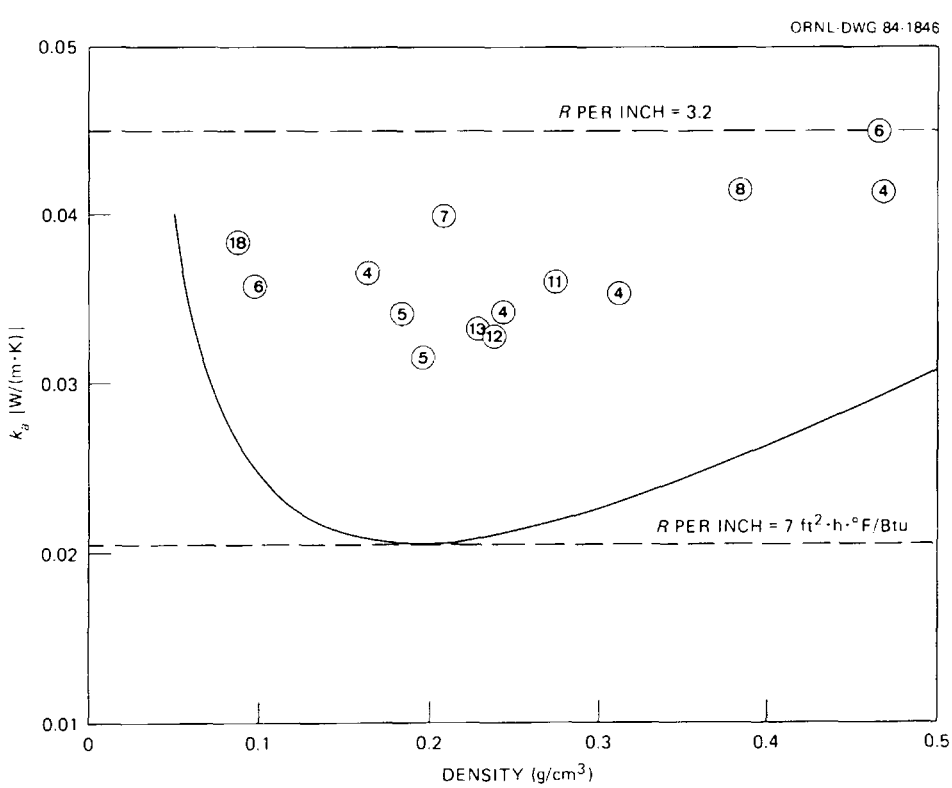

Fig. 13. Apparent thermal conductivity at 300 K and atmospheric pressure as a function of density for inexpensive commercial materials. The curve for Eq. (36) is included.

have larger nominal particle sizes (30 to 300 nm in diameter), and some are not pure silica but contain impurities of Fe_2O_3 and carbon. The k_a values are about 0.01 to 0.02 W/(m·K) larger than given by Eq. (36), which describes the very fine and pure silica powders. The results for Material 4 (SiO_2 Selma Gray) appear to show a minimum k_a near 0.034 W/(m·K) and 0.25 g/cm^3 as suggested by the model.

Apparent thermal conductivity for six powders was measured as a function of pressure with ORNL-3. Curves showing the k_a trend for the fine powders as a function of pressure at two temperatures appear in Fig. 14 along with points for the large-diameter Al_2O_3 particles tested. The results demonstrate the target thermal conductivity of 0.0072 W/(m·K) (R per inch = 20 ft^2·h·°F/Btu) at pressures below 133 Pa for the fine SiO_2 powders tested. The curves in Fig. 14 show that a thermal conductivity of 0.0144 W/(m·K) (R per inch = 10 ft^2·h·°F/Btu) is achievable with the powders tested at pressures in the range 1.3×10^2 to 1.3×10^3 Pa.

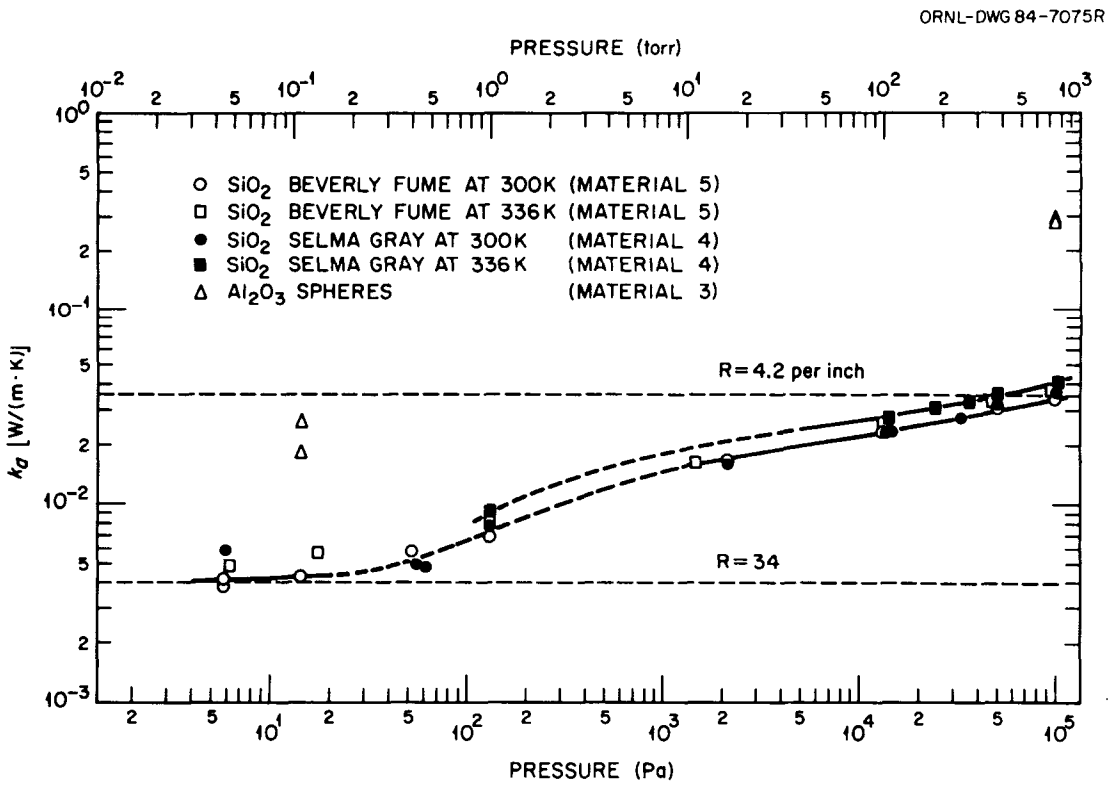

Fig. 14. Measured apparent thermal conductivities of five types of fine particles as a function of interstitial gas pressure.

CONCLUSIONS AND RECOMMENDATIONS

The heat transfer analysis presented in this report shows that apparent thermal conductivities as low as 0.0072 W/(m·K) (R per inch = 20 ft^2·h·°F/Btu) can be achieved by combinations of small particles and reduced pressures. Very low k_a or high R-values are attained by achieving large values for the ratio of the mean free path in the gas phase to particle diameter L_g/d and large values for the structural parameter A. If the gas phase pressure is atmospheric, then an L_g/d greater than 100 is required to achieve k_a < 0.0072 W/(m·K) at 300 K. Reduction of k_r has little effect on k_a at 300 K because the radiative component is calculated to be less than 10% of the total heat transfer except for the smallest F_s considered.

Apparent thermal conductivities in the range 0.0072 to 0.0144 W/(m·K) at 300 K and atmospheric pressure are predicted for attainable ranges of L_g/d and F_s. Experimental measurements on 0.0070-μm SiO_2 powder at 300 K and atmospheric pressure show a minimum k_a of about 0.021 W/(m·K) (R per inch = 6.9 ft^2·h·°F/Btu) at an F_s of about 0.1.

The theoretical analysis and experimental data both demonstrate that high thermal resistance can be attained with evacuated fine powders. Thermal conductivities as low as 0.00865 W/(m·K) (R per inch = 16.7 ft^2·h·°F/Btu were obtained on the evacuated rectangular panels tested. Thermal conductivities below the target value 0.0072 W/(m·K) were observed for fine powders at pressures below 100 Pa.

The theoretical and experimental results presented in this report suggest that a target k_a = 0.0144 W/(m·K) (R per inch = 10 ft^2·h·°F/Btu can be achieved at 300 K and atmospheric pressure by use of very small diameter particles and reduction of radiative transfer as much as possible. The target k_a = 0.0072 W/(m·K) (R per inch = 20 ft^2·h·°F/Btu) is achievable with fine particles and a moderate vacuum.

The results obtained are therefore encouraging. Additional understanding of heat transfer through powders would result from a direct linking of experimental results with a theoretical model. A measurement

of the heat transfer through rectangular samples of fine powders as a function of F_s and pressure would permit the structure parameters L_g/d and A to be determined.

A rectangular measurement system or the existing radial flow apparatuses can be used to expand the search for the optimum F_s and radiation-blocking particle mixtures. Optimum conditions for high thermal resistance need to be determined for low-cost commercially available powders. Once this is achieved attention can be turned to improving processes for the manufacture of powders and methods for assuring that the resultant insulations will retain high thermal resistance for the life of the appliance.

ACKNOWLEDGMENTS

The authors are grateful for the guidance and patience of three Program Managers, V. O. Haynes and F. C. Chen of the Energy Division at the Oak Ridge National Laboratory and R. Fiskum of the Energy Conversion Equipment Branch of the Department of Energy. It is a pleasure to acknowledge the early project assistance of J. P. Moore, formerly of the Metals and Ceramics Division of ORNL, and now with the Advanced Laser Isotope Separation Division of the Oak Ridge Gaseous Diffusion Plant. The measurement systems he selected functioned well on small samples. We would like to thank Frank E. Ruccia, A. D. Little, Inc., for advice during the course of the project.

This project evaluated the potential usefulness of available materials that were provided by several commercial interests. We are particularly appreciative of the following for their cooperation:

Alamet (R. D. Jenkins)
Cabot Corporation (H. Cockrane)
Degussa (T. Bowerton)
Elkem Chemicals (C. E. Broadwine)
L'Air Liquide (J. Y. Faudou and J. Ginebre)
Foote Mineral (C. Shuckers)
Ohio Ferroalloys Corporation (O. A. Savage)
Reynolds Metal Company (T. Givens)

The authors thank R. N. Lyon and G. E. Courville for reviewing the draft report. It is a pleasure to acknowledge the help of a number of people who assisted the authors in preparing this report: Sharon Robinson of the Chemical Engineering Department of Tennessee Technological University for her careful typing of several drafts of the report, Sigfred Peterson and Irene Brogden for their technical editing efforts, and D. L. LeComte and the Reports Office Staff of the Metals and Ceramics Division for expediting the report.

REFERENCES

1. W. T. Lawrence and F. E. Ruccia, *Development of Advanced Insulation for Appliances. Task I Report*, ORNL/Sub-81/13800/1, June, 1981.

2. J. D. Verschoor and P. Greebler, "Heat Transfer by Gas Conduction and Radiation in Fibrous Insulations," *Trans. Am. Soc. Mech. Engr.* 74, 961–68 (1952).

3. P. E. Glaser et al., *Thermal Insulation Systems*, NASA SP 5207, National Aeronautics and Space Administration, 1967.

4. A. W. Pratt, "Heat Transmission in Low Conductivity Materials," pp. 301–405 in *Thermal Conductivity*, vol.1, ed. R. P. Tye, Academic Press, London, 1969.

5. H. M. Strong, F. P. Bundy, and H. P. Bovenkerk, "Flat Panel Vacuum Thermal Insulation," *J. Appl. Phys.* 31, 39–50 (1960).

6. F. W. Sears, *Thermodynamics, the Kinetic Theory of Gases, and Statistical Mechanics*, 2d ed., Addison-Wesley, Reading, Mass. 1953, p. 251.

7. P. Pellaux-Gervais and D. Goumy, "Insulating Material with Low Thermal Conductivity, Formed of a Compacted Granular Structure," U.S. patent 4,159,359 (assigned to L'Air Liquide, Paris, France), June 26, 1979.

8. C. G. Bankvall, "Natural Convective Heat Transfer in Permeable Insulation," pp. 73–81 in *Thermal Transmission Measurements of Insulation*, ASTM STP 660, ed. R. P. Tye, American Society for Testing and Materials, Philadelphia, 1978.

9. E. R. Lapwood, "Convection of a Fluid in Porous Medium," *Proc. Cambridge Philos. Soc.* 44, 508–21 (1948).

10. R. A. Crane, R. I. Vachon, and M. S. Khader, "Thermal Conductivity of Granular Materials — A Review," pp. 109–23 in *Proceedings of the 7th Symposium on Thermophysical Properties*, American Society of Mechanical Engineers, New York, 1977.

11. A. V. Luikov et al., "Thermal Conductivity of Porous Systems," *Int. J. Heat Mass Transfer* 11, 117–40 (1968).

12. D. B. Rogers and J. W. Williamson, "Thermal Characteristics of Gas Filled Fiber Powder Insulation Systems," pp. 317–23 in *Thermal Conductivity 15*, ed. V. V. Mirkovich, Plenum Press, 1978.

13. S. S. Kistler, "The Relationship Between Heat Conductivity and Structure in Silica Aerosol," *J. Phys. Chem.* 39, 79–85 (1935).

14. D. P. DeWitt, *Handbook of the Optical, Thermal and Mechanical Properties of Six Polycrystalline Dielectric Materials*, Report 19, Thermophysical Properties Research Center, Lafayette, Ind., 1972.

15. R. Siegel and J. R. Howell, *Thermal Radiation Heat Transfer*, 2d ed., McGraw-Hill, New York, 1972, p. 413.

16. M. Kerker, *The Scattering of Light*, Academic Press, New York, 1969, pp. 39–50.

17. M. Q. Brewster and C. L. Tien, "Radiative Transfer in Packed Fluidized Beds: Dependent Versus Independent Scattering," *J. Heat Transfer* 104, 573–79 (1982).

18. H. C. Hottel et al., "Optical Properties of Coatings. Effect of Pigment Concentration," *AIAA J.* 9, 1895–98 (1970).

19. R. J. Champetier and G. J. Friese, *Use of Polished Fused Silica to Standardize Directional Polarized Emittance and Reflectance Measurements in the Infrared*, SAMSO-TR-202, The Aerospace Corporation, El Segundo, Calif., 1974

20. D. E. Gray (coord. ed.), *American Institute of Physics Handbook*, 3d ed., McGraw-Hill, New York, 1972, pp. 6–28.

21. P. J. Foster and C. R. Howarth, "Optical Constants of Carbons and Coals in the Infrared," *Carbon* 6, 719–29 (1968).

22. M. N. Ozisik, *Radiative Transfer*, Wiley Interscience, New York, 1973, pp. 316–25.

23. R. Siegel and J. R. Howell, *Thermal Radiation Heat Transfer*, 2d ed., McGraw-Hill, New York, 1972, p. 637.

24. R. Siegel and J. R. Howell, *Thermal Radiation Heat Transfer*, 2d ed., McGraw-Hill, New York, 1972, pp. 739–46.

25. J. P. Moore, D. L. McElroy, and S. H. Jury, *A Technique for Measuring the Apparent Thermal Conductivity of Flat Insulations*, ORNL/TM-6494, October 1979; also *Thermal Conductivity* 17, 727–35 (1983).

26. D. L. McElroy et al., "A Flat Insulation Tester That Uses an Unguarded Nichrome Screen Wire Heater," presented at Forum on the Guarded Hot Plate and Heat Flow Meter State of the Art, Quebec, Canada, Oct. 7–8, 1982.

27. R. S. Graves, D. W. Yarbrough, and D. L. McElroy, "Apparent Thermal Conductivity Measurements by an Unguarded Technique," presented at 18th International Thermal Conductivity Conference, Rapid City, S. Dak., Oct. 3–5, 1983.

28. G. L. Copeland et al., "Insulations with Low Thermal Conductivity," presented at 18th Thermal Conductivity Conference, Rapid City, S. D., Oct. 3–5, 1983.

29. W. D. Turner, D. C. Elrod, and I. I. Siman-Tov, *HEATING5 - An IBM 360 Heat Conduction Program*, ORNL/CSD/TM-15, March 1977.

30. T. G. Godfrey, D. L. McElroy, and Z. L. Ardary, "Thermal Conductivity of Oriented Fibrous Carbon Insulation from 300 to 1300 K in Nitrogen and Argon at One Atmosphere," *Nucl. Technol.* 22, 94–107 (1974).

Appendix A

BRIEF DESCRIPTION OF CONCEPTS FOR PROVIDING HIGH *R*-VALUES

This appendix contains a summary of the insulation concepts identified in the report by Lawrence and Ruccia,* which contains a discussion of each system. Table A.1 summarizes the key material properties, and Table A.2 lists related system information.

*W. T. Lawrence and F. E. Ruccia, *Development of Advanced Insulation for Appliances. Task I Report*, ORNL/Sub-81/13800/1, June, 1981.

Table A.1. Properties for insulation concepts studied by A. D. Little

	Material	Potential *R*-value per inch ($ft^2 \cdot h \cdot °F/Btu$)	Maximum temperature (°C)	Bulk density (kg/m^3)
I.	Polyurethane closed-cell foam	8	65	32–48
II.	Phenolic open-cell foam	8	120	32–48
IV.	Phenolic open-cell foam	15	120	38–48
V-1.	Min K-1400	14	>315	320
V-2.	Fumed SiO_2 powder, compressed	20	>315	240
VI.	Perlite powder	20	>315	144
VII.	Ceramic fiber	20	>315	192
VIII.	Multilayer shields and spacers	556	200	256
IX.	Hollow glass microspheres	15	>315	104
X.	Perlite powder and polyurethane foam	>20	65	112
XI.	Multilayer insulation and foam	>20	65	40
XII.	Perlite and NEMA-GID honeycomb composite	>20	>200	160
A.	Linde vacuum insulation	33	65	32
B.	Linde vacuum insulation	47.6	232	192
C.	Linde vacuum insulation	72.5	482	320
D.	Linde vacuum insulation	167	482	24

Source: W. T. Lawrence and F. E. Ruccia, *Development of Advanced Insulation for Appliances. Task I Report*, ORNL/Sub-81/13800/1, June, 1981.

Table A.2. System information for insulation concepts studied

Material	Relative cost	Interstitial gas pressure (Pa)	Compression from load of 0 to 1×10^5 Pa (%)	Leak detection (std cm^3/s)
I	1.0	1.01×10^5	10	
II	2.0	1.01×10^5	10	10^{-5}
IV	2.5	1.3	10	10^{-9}
V-1	487	1.01×10^5	10	10^{-5}
V-2	22	1.01×10^5	*a*	
VI	1.0	13.3	11	10^{-8}
VII	51	1.33×10^{-2}	10	10^{-11}
VIII	36	1.33×10^{-3}	10	10^{-12}
IX	4	1.33×10^{-4}	10	10^{-13}
X	1.5	13.3	10	10^{-8}
XI	3.5	1.33×10^{-3}	10	10^{-12}
XII	3.0	13.3	10	10^{-8}
A		0.133–13.3	1.5	10^{-10}
B		0.133–13.3	10	10^{-10}
C		0.133–13.3	10	10^{-10}
D		0.133–0.665		10^{-10}

[a]Not applicable.

Appendix B

TABULATION OF $E(\lambda)$ FOR FOUR PARTICLES AND VALUES FOR $\overline{C}$

Table B.1. $E(\lambda)$ and $\overline{C}_{Si}$ for 0.0070-μm-diam silica particles

λ (μm)	$E(\lambda)^a$ (m^{-1})	λ (μm)	$E(\lambda)$ (m^{-1})
2.0	0.058	14.5	4,444.5
2.5	0.023	15.0	4,813.3
3.0	3.33	15.5	5,752.4
3.5	2.87	16.0	7,266.0
4.0	15.3	16.5	9,290.4
4.5	688.4	17.0	11,658.2
5.0	631.0	17.5	14,242.7
5.5	1,956.9	18.0	16,989.9
6.0	1,477.0	18.5	20,266.8
6.5	1,417.1	19.0	26,239.9
7.0	2,390.6	19.5	39,500.6
7.5	4,585.3	20.0	79,280.1
8.0	36,453.4	20.5	174,387.1
8.5	197,249.2	21.0	39,807.5
9.0	92,080.7	21.5	25,915.4
9.5	32,423.1	22.0	20,367.5
10.0	10,471.2	22.5	16,721.9
10.5	6,903.6	23.0	13,238.2
11.0	8,639.3	23.5	10,394.5
11.5	12,345.9	24.0	8,258.6
12.0	17,189.9	24.5	6,677.2
12.5	20,965.1	25.0	5,547.5
13.0	12,511.5	25.5	4,738.2
13.5	6,241.8	26.0	4,086.6
14.0	4,374.8		

$^a F_s = 0.10$

T_m (K)	$\overline{C}_{Si}$ (m^{-1})
300.0	0.2231×10^6
400.0	0.2298×10^6
500.0	0.2037×10^6
600.0	0.1696×10^6
700.0	0.1380×10^6
800.0	0.1117×10^6
900.0	0.9071×10^5

Table B.2. $E(\lambda)$ and $\overline{C}_p$ for 1-μm-diam silica particles

λ (μm)	$E(\lambda)^a$ (m^{-1})	λ (μm)	$E(\lambda)$ (m^{-1})
2.0	4,736.5	14.5	97,581.9
2.5	5,051.3	15.0	50,379.5
3.0	5,961.4	15.5	26,727.0
3.5	7,464.2	16.0	14,464.0
4.0	9,489.0	16.5	8,085.8
4.5	11,860.0	17.0	5,412.0
5.0	14,437.3	17.5	3,355.3
5.5	17,155.5	18.0	3,631.8
6.0	20,372.8	18.5	2,348.3
6.5	26,256.0	19.0	1,801.8
7.0	39,333.0	19.5	2,463.4
7.5	78,252.9	20.0	4,547.2
8.0	180,040.6	20.5	34,383.8
8.5	41,964.0	21.0	171,816.2
9.0	27,396.6	21.5	133,851.6
9.5	21,518.7	22.0	45,694.9
10.0	17,603.0	22.5	14,337.8
10.5	13,886.8	23.0	8,607.9
11.0	10,871.4	23.5	9,984.7
11.5	8,615.8	24.0	13,607.3
12.0	6,951.8	24.5	18,417.5
12.5	5,765.2	25.0	22,534.2
13.0	4,915.6	25.5	13,610.8
13.5	4,232.8	26.0	6,810.1
14.0	4,732.8		

[a] $F_s = 0.10$

T_m (K)	$\overline{C}_p$ (m^{-1})
300.0	0.2399×10^6
400.0	0.2522×10^6
500.0	0.2369×10^6
600.0	0.2227×10^6
700.0	0.2203×10^6
800.0	0.2294×10^6
900.0	0.2461×10^6

Table B.3. $E(\lambda)$ and $\overline{C}_p$ for 10-μm-diam silica particles

λ (μm)	$E(\lambda)^a$ (m^{-1})	λ (μm)	$E(\lambda)$ (m^{-1})
2.0	31,245.1	14.5	47,711.1
2.5	43,373.3	15.0	39,426.1
3.0	30,988.9	15.5	32,728.3
3.5	26,024.7	16.0	27,503.5
4.0	40,759.5	16.5	24,471.6
4.5	51,990.5	17.0	22,791.7
5.0	58,443.4	17.5	21,504.7
5.5	53,810.3	18.0	20,109.0
6.0	41,757.5	18.5	18,953.9
6.5	23,991.6	19.0	19,912.5
7.0	5,437.2	19.5	24,319.7
7.5	5,426.2	20.0	34,314.4
8.0	28,732.2	20.5	58,407.7
8.5	37,805.3	21.0	51,359.2
9.0	50,675.0	21.5	46,511.5
9.5	41,271.2	22.0	45,866.7
10.0	43,046.3	22.5	46,279.2
10.5	40,858.2	23.0	47,734.9
11.0	53,395.9	23.5	50,355.8
11.5	51,780.9	24.0	53,765.8
12.0	47,604.5	24.5	57,341.8
12.5	46,873.9	25.0	60,672.2
13.0	51,589.8	25.5	63,652.8
13.5	61,121.2	26.0	66,318.1
14.0	57,157.9		

[a] $F_s = 0.10$

T_m (K)	$\overline{C}_p$ (m^{-1})
300.0	0.3397×10^6
400.0	0.3591×10^6
500.0	0.3695×10^6
600.0	0.3756×10^6
700.0	0.3778×10^6
800.0	0.3763×10^6
900.0	0.3716×10^6

Table B.4. $E(\lambda)$ and $\overline{C}_p$ for 0.020-μm-diam carbon particles

λ (μm)	$E(\lambda)^a$ (m^{-1})	λ (μm)	$E(\lambda)$ (m^{-1})
2.0	217,084.6	14.5	7,569.4
2.5	156,485.9	15.0	7,317.1
3.0	122,555.6	15.5	7,081.1
3.5	98,502.7	16.0	6,859.8
4.0	80,711.4	16.5	6,651.9
4.5	67,937.1	17.0	6,456.3
5.0	57,470.6	17.5	6,271.8
5.5	48,387.2	18.0	6,097.6
6.0	41,598.8	18.5	5,932.8
6.5	35,230.7	19.0	5,776.7
7.0	32,164.9	19.5	5,628.5
7.5	34,167.0	20.0	5,487.8
8.0	26,828.7	20.5	5,354.0
8.5	20,304.0	21.0	5,226.5
9.0	15,689.5	21.5	5,105.0
9.5	12,996.0	22.0	4,988.9
10.0	10,975.8	22.5	4,878.1
10.5[b]	10,453.2	23.0	4,772.0
11.0	9,979.0	23.5	4,670.5
11.5	9,544.2	24.0	4,573.2
12.0	9,146.5	24.5	4,479.8
12.5	8,780.6	25.0	4,390.2
13.0	8,442.9	25.5	4,304.2
13.5	8,130.2	26.0	4,221.4
14.0	7,839.8		

[a] $F_s = 0.10$

[b] Results for $\lambda > 10$ μm were obtained by use of the complex refractive index at 10 μm.

T_m (K)	$\overline{C}_p$ (m^{-1})
300.0	0.1208×10^6
400.0	0.2095×10^6
500.0	0.3128×10^6
600.0	0.4244×10^6
700.0	0.5384×10^6
800.0	0.6478×10^6
900.0	0.7459×10^6

Appendix C

THERMAL CONDUCTIVITY DATA OBTAINED WITH ORNL-3 AND ORNL-4

Table C.1. k_a Obtained with radial heat flow apparatus ORNL-3

(Note: 1 mm Hg = 133.3 Pa)

	Material[a]	T (K)	P (mm Hg)	Medium	k_a [W/(m·K)]
3	500-μm Al_2O_3 spheres; density, 2.277 g/cm^3	297.10	760	Air	0.279
		297.76	760		0.280
		313.33	760		0.290
		332.69	760		0.310
		332.70	760		0.310
		313.45	750	N_2	0.295
		313.60	437		0.280
		313.35	263		0.300
3	500-μm Al_2O_3 spheres; density, 2.265 g/cm^3	316.18	0.125	Air	0.0178
		316.34	0.115		0.0170
		299.92	0.110		0.0266
		299.70	0.110		0.0185
1	0.0070-μm Cab-O-Sil S-17; density, 0.0807–0.0886 g/cm^3;[b] F_s, 0.037–0.040	313.04	756	N_2	0.0303
		334.02	760		0.0332
		299.15	760		0.0287
		300.06	0.096	Air	0.00604
		313.73	0.094		0.00683
16	Mixture, 25 vol % Cab-O-Sil S-17,75 vol % 3M microspheres, density, 0.097 g/cm^3	315.8	760	N_2	0.0372
		301.5	760		0.0360
17	Perlite; density, 0.146 g/cm^3	301.09	760	N_2	0.0561
		313.39	760		0.0581
		333.07	760		0.0621
18	3M microspheres, 100-μm; density, 0.0826 g/cm^3	299.57	760	N_2	0.0382
		313.23	760		0.0396
		332.88	760		0.0417
	density, 0.0887 g/cm^3[c]	299.71	743	N_2	0.0378
		313.51	760		0.0400
		333.98	760		0.0422
		299.90	760		0.0387
		300.68	0.125	Air	0.00632
		312.28	0.115		0.00602
		333.15	0.082		0.00438

Table C.1 (continued)

	Material[a]	T (K)	P (mm Hg)	Medium	k_a [W/(m·K)]
4	SiO_2 Selma Gray; density, 0.361 g/cm^3 F_s, 0.163	310.43	0.043	Air	0.00544
		336.27	0.055		0.00614
		298.35	0.048		0.00486
		299.51	0.043		0.00503
		300.09	760	N_2	0.0369
		299.00	252		0.0279
		298.15	101		0.0230
		301.98	385		0.0317
		300.43	111		0.0238
		335.80	760		0.0396
		336.22	385		0.0349
		336.70	276		0.0336
		335.94	187		0.0308
		336.50	107		0.0275
		299.63	0.045	Air	0.00590
		337.78	17	N_2	0.0165
		337.78	16		0.0166
		301.02	16		0.0163
		300.75	1		0.00798
		336.17	1		0.00922
5	SiO_2 Beverly mixed fume; density, 0.1809 g/cm^3; F_s, 0.0819	300.22	0.044	Air	0.00384
		315.43	0.046		0.00428
		335.68	0.047		0.00487
		336.11	760	N_2	0.0366
		336.87	377		0.0343
		338.86	96		0.0258
		336.88	11		0.0158
		334.83	1		0.0086
		336.71	0.133		0.0057
		300.08	0.110		0.0043
		300.53	0.044	Air	0.0042
		300.11	745	N_2	0.0342
		300.19	381		0.0309
		300.22	101		0.0232
		300.10	15.7		0.0166
		300.30	1		0.00685
		299.99	0.4		0.00578
		300.03	0.045		0.00387

[a]Additional information about materials is in Appendix D. Identification numbers match those in Tables 16 an 17.

[b]Initial and final densities were recorded.

[c]Density was measured before 21-d anneal at 450°C and vacuum.

Table C.2. k_a Obtained with radial heat flow apparatus ORNL-4 (measured at atmospheric pressure)

	Material[a]	T (K)	Medium	k_a [W/(m·K)]
1	7.0-nm Cab-O-Sil S-17; density, 0.280 g/cm^3; F_s, 0.127	298.4	Air	0.0229
		312.8	Air	0.0235
		323.6	Air	0.0240
		333.1	Air	0.0246
		327.2	Air	0.0242
2	Degussa R-974 Aerosil SiO_2; density, 0.366 g/cm^3; F_s, 0.166	298.3	Air	0.0250
		312.5	Air	0.0256
		322.9	Air	0.0265
		328.5	Air	0.0269
		333.5	Air	0.0273
		328.4	Air	0.0268
		333.5	Air	0.0273
		322.9	Air	0.0265
		299.5	Air	0.0250
1	7.0-nm Cab-O-Sil S-17; density, 0.099 g/cm^3; F_s, 0.045	297.9	N_2	0.0232
		307.2	N_2	0.0240
		315.8	N_2	0.0247
		324.4	N_2	0.0255
		334.2	N_2	0.0265
	7.0-nm Cab-O-Sil S-17; density, 0.181 g/cm^3; F_s, 0.082	306.2	N_2	0.0217
		316.0	N_2	0.0224
		324.5	N_2	0.0230
		296.7	N_2	0.0211
		333.4	N_2	0.0237
	7.0-nm Cab-O-Sil S-17; density, 0.280 g/cm^3; F_s, 0.127	333.2	N_2	0.0243
		323.2	N_2	0.0233
		313.8	N_2	0.0227
		300.8	N_2	0.0219
	7.0-nm Cab-O-Sil S-17; density, 0.496 g/cm^3; F_s, 0.225	305.4	N_2	0.0416
		315.5	N_2	0.0429
		325.3	N_2	0.0433
		332.4	N_2	0.0440
		328.9	N_2	0.0436
		298.2	N_2	0.0417
3	500-μm Al_2O_3; density, 2.395 g/cm^3	294.7	N_2	0.2709
		309.3	N_2	0.2786
		323.8	N_2	0.2834
		333.6	N_2	0.2879
4	Selma Gray SiO_2 powder; density, 0.2424 g/cm^3; F_s, 0.110	300.3	N_2	0.0343
		316.3	N_2	0.0355
		331.5	N_2	0.0368
		300.6	N_2	0.0343

Table C.2. (continued)

	Material[a]	T (K)	Medium	k_a [W/(m·K)]
	Selma Gray SiO_2 powder; density, 0.3122 g/cm^3; F_s, 0.142	301.2	N_2	0.0356
		314.5	N_2	0.0365
		332.1	N_2	0.0375
		303.7	N_2	0.0361
	Selma Gray SiO_2 powder; density, 0.4679 g/cm^3; F_s, 0.213	300.9	N_2	0.0416
		338.3	N_2	0.0437
5	Beverly mixed fume 85 vol % SiO_2 with iron and carbon; density, 0.195 g/cm^3	300.6	N_2	0.0319
		339.0	N_2	0.0350
6	Fumed SiO_2 Ohio Ferroalloys; density, 0.4643 g/cm^3; F_s, 0.211	301.1	N_2	0.0451
		334.7	N_2	0.0476
7	SiO_2 Selma White; density, 0.2089 g/cm^3; F_s, 0.095	301.6	N_2	0.0400
		334.6	N_2	0.0431
8	SiO_2 Reynolds fume dust 1; density, 0.382 g/cm^3; F_s, 0.174	300.8	N_2	0.0415
		314.1	N_2	0.0427
		335.2	N_2	0.0442
9	20-200-μm Cenospheres; density, 0.3678 g/cm^3	298.9	N_2	0.1114
		317.3	N_2	0.1151
		333.5	N_2	0.1199
10	DeGussa Aerosil 500; density, 0.0539 g/cm^3; F_s, 0.025	300.4	N_2	0.0260
		318.0	N_2	0.0279
		335.1	N_2	0.0302
	DeGussa Aerosil 500; density, 0.0796 g/cm^3; F_s, 0.035	299.9	N_2	0.0231
		317.7	N_2	0.0248
		327.9	N_2	0.0259
		336.6	N_2	0.0259
		299.3	N_2	0.0231
11	Microsilica Elkem chemical, 95 % SiO_2; density, 0.273 g/cm^3	300.0	N_2	0.0359
		318.2	N_2	0.0369
		335.7	N_2	0.0382
12	Microsilica Elkem chemical, 88% SiO_2; density, 0.238 g/cm^3	300.8	N_2	0.0329
		318.2	N_2	0.0339
		336.2	N_2	0.0352
13	Elkem chemical, 88% SiO_2 and 12% Fe_2O_3; density, 0.232 g/cm^3	299.9	N_2	0.0329
		318.1	N_2	0.0342
		336.3	N_2	0.0358

[a]Identification numbers match those used in Appendix D and Tables 16 through 18.

Appendix D

SOURCES OF MATERIALS TESTED

Table D.1. Sources of materials tested

Item	Identification and source
1	Cab-O-Sil S-17, a fumed SiO_2 with an average particle size of 0.007 μm Mozel Chemical Products Company 1797 Florida Street Memphis, TN 38109
2	Degussa R974 Degussa, Inc., Pigments Div. Route 46 at Hollister Road Teterboro, NJ 07608
3	Aluminum oxide microspheres General Atomic Company San Diego, CA
4	Amorphous silica Alabama Metallurgical Corp. (ALAMET) P.O. Box 348 Selma, AL 36701-0348
5	Amorphous silica Interlake, Inc. Globe Metallurgical Division Beverly, OH
6	Amorphous silica Ohio Ferroalloys Corporation P.O. Box 68 Mt. Meigs, AL 36057
7	Amorphous silica Alabama Metallurgical Corporation (ALAMET) P.O. Box 348 Selma, AL 36701-0348
8	Amorphous silica Reynolds Metals Company P.O. Box 191 Listerhill, AL 35660
9	Cenospheres Obtained from M. A. Karnitz, Energy Division, ORNL

Table D.1 (continued)

10	Degussa Aerosil 500 Degussa, Inc., Pigments Division Route 46 at Hollister Road Teterboro, NJ 07608
11, 12, and 13	Amorphous silica mixtures Elkem Chemicals, Inc. Park West Office Center Building One P.O. Box 177 Pittsburgh, PA 15230
Component of 14 and 15	Carbon black, Philblack S212 Phillips Chemical Company Division of Phillips Petroleum Company 3090 W. Market St. Akron, OH 44313
17	Perlite Obtained from local retail store
18	3M microspheres 3M Company, Special Enterprises Deptartment 3M Center, St. Paul, MN 55144

ORNL/CON-159
Distribution
Category UC-95d

INTERNAL DISTRIBUTION

1–2. Central Research Library
3. Document Reference Section
4–5. Laboratory Records Department
6. Laboratory Records, ORNL RC
7. ORNL Patent Section
8. E. E. Bloom
9. A. J. Caputo
10. J. J. Carbajo
11. R. S. Carlsmith
12. J. A. Carpenter, Jr.
13–18. F. C. Chen
19. R. E. Clausing
20–24. G. L. Copeland
25–29. G. E. Courville
30. F. A. Creswick
31. W. P. Eatherly
32. L. C. Emerson
33–37. H. A. Fine
38. A. T. Fisher
39. W. Fulkerson
40. T. G. Godfrey, Jr.
41–45. R. S. Graves
46. R. J. Gray
47. V. O. Haynes
48. H. W. Hoffman
49. R. R. Judkins
50. G. E. Kamp
51. W. J. Lackey
52–61. T. S. Lundy
62. R. N. Lyon
63. J. F. Martin
64–68. M. C. Matthews
69–73. D. L. McElroy
74. J. W. Michel
75. R. E. Minturn
76. W. R. Mixon
77. J. P. Moore
78. R. E. Pawel
79. M. W. Rosenthal
80. A. C. Schaffhauser
81. J. O. Stiegler
82. V. J. Tennery
83–85. P. T. Thornton
86–90. T. W. Tong
91–95. F. J. Weaver
96. J. R. Weir, Jr.
97. R. O. Williams
98. D. W. Yarbrough
99. R. J. Charles (Consultant)
100. R. E. Goodson (Consultant)
101. T. R. LaPorte (Consultant)
102. Alan Lawley (Consultant)
103. F. R. Kalhamma (Consultant)
104. T. B. Massalski (Consultant)
105. L. I. Moss (Consultant)
106. J. C. Williams (Consultant)
107. K. M. Zwilsky (Consultant)

EXTERNAL DISTRIBUTION

108. P. R. ACHENBACH, 1322 Kurtz Road, McLean, VA 22101

109. ALAMET, P.O. Box 348, Selma, AL 36702
R. D. Jenkins

110. ALTERNATE ENERGY INSTITUTE, P.O. Box 3100, Estes Park, CO 80517
S. Mitchel

111. APPLEGATE INSULATION SYSTEMS, P.O. Box 292, Okemos, MI 48864

T. Applegate

112. BABCOCK & WILCOX COMPANY, Alliance Research Center, 1562 Beeson Street, Alliance, OH 44601

H. W. Wahle

113. BENSON WOODWORKING COMPANY, Inc., Pratt Road, Alstead Center, NH 03602

T. H. Benson

114. JOHN M. BRADLEY, Eaglehead Road, Manchester, MA 01944

115—116. BROWN, BOVERI, & CIE AG, Eppenheimer Strasse 82, 6900 Heidelberg, West Germany

H. Reiss
B. Ziegenbein

117. CABOT CORPORATION, CAB-O-OSIL Division, P.O. Box 188, Tuscola, IL 61953

H. Cochrane

118. CERTAIN-TEED PRODUCTS CORP., P.O. Box 860, Valley Forge, PA 19482

J. F. Kimpflen

119. CERTAIN-TEED CORPORATION, 1400 Union Meeting Rd., Blue Bell, PA 19422

D. J. McCaa

120. CHALMERS UNIVERSITY OF TECHNOLOGY, Department of Physics, S-412 96, Göteborg, Sweden

S. Gustafsson

121. DAVID TAYLOR NAVAL SHIP R&D CENTER, Mail Code 2722, Annapolis Laboratory, Annapolis, MD 21402

Bao Hwang

122—123. DEGUSSA AG, POSTFACH 1345, Rodenbacher Strasse 4 D-6450 Hanau, West Germany

H. Ferch
M. Ettlinger

124—125. DEGUSSA CORPORATION, Route 46 Hollister Road, Teterboro, NJ 07608

T. Bowerman
K. C. Cwick

126. DOW CHEMICAL COMPANY, Granville Research Center, P.O. Box 515, Granville, OH 43023

D. Greason

127—128. DYNATECH R/D COMPANY, 99 Erie Street, Cambridge, MA 02139

A. O. Desjarlais
R. P. Tye

129. ELKEM CHEMICALS, INC., P.O. Box 177, Pittsburgh, PA 15230

C. E. Broadwine

130. ENERGY SPECTRUM, P.O. Box 4046, Madison, WI 53711

L. G. Nordling

131. FIBERGLAS CANADA, INC., P.O. Box 3005, Sarnia, Ontario, Canada N7T 7M6

N. M. Cameron

132. FOOTE MINERAL, Ferroalloys Division, Route 100, Exton, PA 19341

C. Shuckers

133—137. GENERAL ELECTRIC CO., Corporate Research and Development, P.O. Box 43, Schnectady, NY 12301

N. Abuaf
H. Jaster
B. Kermati
G. A. Slack
W. J. Ward

138—144. GENERAL ELECTRIC CO., Appliance Park, 35-113, Louisville, KY 40225

J. Ackley
R. W. Barito
K. L. Downs
B. Horvay
M. McCormick
L. McIntosh
J. Ziegler

145. GEOSCIENCE LTD., 410 S. Cedros Ave., Solana Beach, CA 92075

H. F. Poppendick

146. IMA INSULATION COMPANY, 2902 Brisban St., Harrisburg, PA 17111

G. S. Bowman

147. INSTITUTO DI FISICA TECHNICA, Facolta Ingegneria-Univ Padova, Via f. Marzolo N9, Padova 35100 Italy

F. DePonte

148—149. L'AIR LIQUIDE, 57 Avenue Carnot, 94500 Champigny, France

J. Y. Faudou
J. Ginebre

150—153. LAWRENCE BERKELEY LABORATORY, University of California, Bldg. 90, Rm. 3058, Berkeley, CA 94720

W. L. Carroll
A. J. Hunt
M. Rubin
C. L. Tien

154. LEGER DESIGNS, P.O. Box 219, New Ipswich, NH 03071

G. Leger

155—157. A. D. LITTLE, INC., Acorn Park, Cambridge, MA 02140

W. T. Lawrence
F. E. Ruccia
P. E. Glazer

158. LOCKHEED PALO ALTO RESEARCH LABORATORY, Dept. 52-32 Bldg. 205, 3251 Hanover St., Palo Alto, CA 94304

G. R. Cunnington

159. LOUISIANA PACIFIC CORP., PABCO INSULATION DIV., 1110 16 Rd, Fruita, CO 81521

F. B. Hutto, Jr.

160. MASSACHUSETTS INSTITUTE OF TECHNOLOGY, Department of Mechanical Engineering, Cambridge, MA 02139

L. R. Glicksman

161. MICROPORE INTERNATIONAL, LTD., Droitwich, Worcestershire, UNITED KINGDOM

J. T. Hughes

162. MINERAL INSULATION MANUFACTURERS ASSOCIATION, 382 Springfield Ave., Summit, NJ 07901

S. H. Cady

163. MINNESOTA ENERGY AGENCY, 980 American Center Building, 150 East Kellogg Boulevard, St. Paul, MI 55101

J. M. O'Neal

164—166. NATIONAL BUREAU OF STANDARDS, DEPARTMENT OF COMMERCE, Gaithersburg, Washington, DC 20234

B. Peavy
F. J. Powell
B. G. Rennex

167. NATIONAL BUREAU OF STANDARD-BOULDER, CYROGENICS DIVISION, INSTITUTE FOR BASIC STANDARDS, Boulder, CO 80303

J. G. Hust

168. NATIONAL INSTITUTE OF BUILDING SCIENCES, 1015 15th Street, NW, Washington, DC 20005

P. M. Greene

169–171. NATIONAL RESEARCH COUNCIL OF CANADA, Montreal Road, Ottawa Ontario K1A OR6, Canada

M. Bomberg
R. Bowen
C. J. Shirtliffe

172–173. OFFICE OF TECHNOLOGY ASSESSMENT, 600 Pennsylvania Ave., SE, Washington, DC 20510

J. H. Gibbons
N. Naismith

174. OHIO FERROALLOYS, P.O. Box 68, Mount Meigs, AL 36057

O. A. Savage

175–176. OWENS-CORNING FIBERGLAS CORP., Technical Center, Box 415, Granville, OH 43023

M. Hollingsworth, Jr.
K. E. Wilkes

177. PENNSYLVANIA STATE UNIVERSITY, Department of Horticulture, 101 Tyson Building, University Park, PA 16802

J. W. White

178. PITTSBURGH CORNING CORP., 800 Presque Isle Drive, Pittsburgh, PA 15239

R. W. Gerrish

179. RENEWABLE TECHNOLOGIES, INC., P.O. Box 4113, Butte, MT 59701

S. Anderson

180. REYNOLDS METAL CO., Sheffield, AL 35660

T. Givens

181. ROCKWOOL INDUSTRIES, INC., P.O. Box 5170, Denver, CO 80217

S. L. Matthews

182. RYERSON POLYTECHNICAL INSTITUTE, Energy Centre, 50 Gould Street, Toronto, Ontario, Canada M5B 1E8

H. Burkhardt

183—184. ST. GOBAIN ISOVER, CENTRE DE RECHERCHES INDUSTRIELLE DE RANTIGNY, 60290 Rantigny, France

Cather Langlais
S. Klarsfeld

185. MAXINE SAVITZ, 5019 Lowell St., N.W., Washington, DC 20014

186. SOLAR AGE, Church Hill, Harrisville, NH 03450

S. B. Bliss

187. SOUTH DAKOTA OFFICE OF ENERGY POLICY, STATE CAPITOL, Pierre, SD 57501

S. M. Wegman

188. STATE OF IDAHO, DEPARTMENT OF WATER RESOURCES, Statehouse, Boise, ID 83720

M. R. McSorley

189. STEVENS INSTITUTE OF TECHNOLOGY, Department of Materials and Metallurgical Engineering, Hoboken, NJ 07030

R. Weil

190. TENNESSEE VALLEY AUTHORITY, 205 Sheraton Building, Chattanooga, TN 37401

D. Lamb

191. TENNESSEE VALLEY AUTHORITY, 1719 West End Building, Nashville, TN 37203

P. A. Rains

192. 3M COMPANY, 23923 Research Drive, P.O. Box 2600, Farmington, MI 48018

J. D. Walraven

193. THERMOBOARD MANUFACTURING CO., P.O. Box 220, Albuquerque, NM 87102

C. M. Jones

194. TUFTS UNIVERSITY, Department of Physics, Medford, MA 02155

H. H. Sample

195. UNION CARBIDE CORP., LINDE DIVISION, Box 44, Tonawanda, NY 14150

J. J. Nowabilski

196. U.S. DEPARTMENT OF HOUSING AND URBAN DEVELOPMENT, 451 7th Street, SW, Washington, DC 20410

M. W. Dizenfeld

197. U.S. NAVAL ACADEMY, DEPARTMENT OF MECHANICAL ENGINEERING, Annapolis, MD 21402

R. C. Wu

198. UNIVERSITY OF CONNECTICUT, DEPARTMENT OF PHYSICS, Storrs, CT 06268

P. G. Klemens

199. UNIVERSITY OF VANDERBILT, DEPARTMENT OF PHYSICS, Nashville, TN 37240

J. W. Williamson

200. UNIVERSITY OF WURZBURG, PHYSICS INSTITUTE, D-8700 Wurzburg, West Germany

J. Fricke

201—202. JIM WALTER RESEARCH CORP., 10301 9th Street, North, St. Petersburg, FL 33702

G. Miller
M. Sherman

203. Robert Wick, 7713 Wilcox, Forest Park, IL 60130

204—211. DOE, CONSERVATION AND RENEWABLE ENERGY, The Forrestal Building, 1000 Independence Ave., Washington, DC 20585

R. J. Fiskum
W. Gerken
Ted Kapus
D. C. Lim
J. P. Millhone
R. Oliver
J. D. Ryan
A. Streb

212—213. DOE, OAK RIDGE OPERATIONS OFFICE, P.O. Box E, Oak Ridge, TN 37830

Office of Assistance Manager for Energy Research and Development
S. S. Waddle

214—467. DOE, TECHNICAL INFORMATION CENTER, OFFICE OF INFORMATION SERVICES, P.O. Box 62, Oak Ridge, TN 37830

For distribution as shown in TID-4500 Distribution Category, UC-95d (Energy Conservation—Buildings and Community Systems)